# Identifying the Mechanisms Behind Radiation Resistance in Treatment Naive Diffuse Midline Glioma Models

Eric Ferguson

A dissertation

submitted in partial fulfillment of the

requirements for the degree of

Doctor of Philosophy

University of Washington

2021

Reading Committee:

Jim Olson, Chair

Nephi Stella

Sandy Bajjalieh

Program Authorized to Offer Degree:

Pharmacology

University of Washington

## ABSTRACT

Identifying the Mechanisms Behind Radiation Resistance in Treatment Naive Diffuse Midline Glioma Models

Eric Ferguson

Chair of the Supervisory Committee:

Jim Olson

Department of Pharmacology

Diffuse Intrinsic Pontine Glioma (DIPG) is a near universally fatal pediatric brain tumor that occurs in the pons and other midline structures. These tumors are characterized by the presence of a unique histone mutation: H3 K27M. This mutation inhibits the polycomb repressive complex 2 (PRC2) and reduces the global H3 K27 trimethylation mark. DIPG is resistant to conventional therapies such as radiation and chemotherapy which contributes to the high mortality rate in DIPG patients. A major challenge to researching DIPG is a lack of tissue available for research models. Due to the sensitive location of DIPG tumors, these tumors cannot be removed by surgery. All current DIPG models are either generated from autopsies or genetically engineered from mice or human stem cells. Currently no drug developed from these research models have translated into a successful clinical therapy. In order to develop a model that more accurately represents to disease state, we developed a protocol to collect biopsies from DIPG patients prior to treatment. Using these treatment naive DIPG biopsy models, we observed similar resistance to radiation therapy compared to how the tumors behaved in the clinic. A key component of the resistance to radiation was the inability of DIPG cells to undergo apoptosis. We found that the pro-apoptotic protein BCL-2 associated X (BAX) was significantly reduced in DIPG compared to other pediatric brain tumors. When radiation sensitive cells were irradiated, they

upregulated BAX but in DIPG this response was significantly reduced. In order to overcome the reduced levels of BAX, we inhibited the pro survival BCL-2 family proteins and found that the pan BCL-2, BCL-xl inhibitor navitoclax was able to sensitize DIPG cells to radiation. We measured the percent of pro-apoptotic cells and found the combination of navitoclax and radiation significantly increase the percent of pro-apoptotic cells in the combination treatment compared to either treatment individually. Future work will focus on why BAX is downregulated in DIPG compared to other pediatric brain tumors. We have identified several transcription factors and epigenetic regulators of BAX that are dysregulated in DIPG. This research has contributed to our understanding of how DIPG resists conventional therapy and may lead to targeted therapies which sensitize DIPG and improve the overall patient survival.

**TABLE OF CONTENTS**

**Chapter 4: Conclusion and Future Direction**

LIST OF FIGURES

## PREFACE

Portions of the test and data from this dissertation are reprinted (adapted) from the following works under fair use and or with permission under the terms of the CC-BY License

1. Vitanza, N.A., et al., *Optimal therapeutic targeting by HDAC inhibition in biopsy-derived treatment-naïve diffuse midline glioma models.* Neuro Oncol, 2020.

## Chapter 1: Introduction to Pediatric Diffuse Midline Glioma and Therapeutic Strategies

### 1.1 Abstract:

Diffuse intrinsic pontine glioma (DIPG), which is now included in the World Health Organization's Diffuse Midline Glioma (DMG) diagnostic category, is a class of pediatric brain stem tumors characterized by unique molecular features and an extremely poor overall prognosis. Due to the diffuse infiltration of these tumors throughout the brainstem, surgical resection is not an option. While chemotherapy has not extended patient survival, radiation has proven to be the only therapy to show a transient response in DIPG, extending median overall survival to approximately 12 months. Because of the aggressive nature of DIPG coupled with treatment challenges, the 5-year survival for patients with DIPG is <1%. This low survival rate has made it imperative that researchers understand the molecular mechanisms that underlie treatment resistance in order to improve the poor prognosis in DIPG patients.

### 1.2 Classification of Pediatric Diffuse Gliomas:

Pediatric tumors in the central nervous system (CNS) are the most common form of solid tumor found in children, with around 3 per 100,000 new cases per year [1]. Among all pediatric tumors, pediatric high-grade glioma (pHGG) is the leading cause of death, with a median overall survival rate of less than one year[2, 3]. Initially, pHGG were grouped with adult high-grade gliomas, despite morphological differences between these two groups [4]. With advances in high throughput genomic sequencing and cluster analysis by DNA methylation profiles, researchers have been able to classify and distinguish pHGG as a molecularly distinct subgroup from adult high-grade gliomas [5].

All gliomas are characterized as tumors which arise from glial or glial progenitor cells such as astrocytes and oligodendrocytes [6, 7]. Early classification of pediatric gliomas was based on distinct histological features as well as tumor location [8]. Gliomas are characterized based on the malignancy

scale, which grades tumor histology on a scale of 1 - 4 based on the abnormality of the tumor compared to healthy tissue. Lower grades are typically more benign, while high grade tumors are more aggressive. High grade pediatric glioma exhibits a diffuse growth pattern which is defined by tumor infiltration into healthy neural tissue [9]. The most prominent anatomical location of pHGG was in the midline structures of the brain, such as the pons and brainstem. The anatomical location, in combination with their diffuse nature, prompted these tumors to be further classified of this subset of pHGG as diffuse intrinsic pontine glioma (DIPG)[10].

In 2012, genomic sequencing of DIPG tumors revealed the presence of a reoccurring mutation to the histone H3 gene. This mutation involved the conversion of lysine 27 to a methionine (H3 K27M) [11, 12]. This mutation was largely absent in adult high-grade gliomas and pHGGs that are not localized within the midline structures [2]. The discovery of these mutant histones, dubbed “oncohistones,” revealed several distinct subtypes of DIPG based on specific mutations and molecular features. DIPG, which contained the H3 K27M mutation, have a significantly worse prognosis, with median overall survival of 9 months and a 2-year survival of less than 1% [13]. A meta-analysis of over 1000 cases of DIPG used molecular driver mutations as well as age, anatomical location, and methylation profiles to define 8 subtypes of DIPG: H3 G34R/V mutant, H3 K27M mutant, H3 wildtype HGG, IDH1 mutant, low-grade glioma like, pleomorphic xanthoastrocytoma (PXA) like and “other” [2]. In 2016, the World Health Organization reclassified all DIPG which contained the H3 K27M mutation as Diffuse Midline Glioma (DMG) [14]. Histone wild type DIPG are still considered pHGG. Although DIPG is no longer the official terminology, it is still used colloquially to refer to pHGG in the brainstem. As researchers continue to study and understand the underlying molecular biology of pHGG, classification of specific subgroups within pHGG will become more accurate, leading to improved targeted therapy and personalized medicine.

### 1.3 H3 K27M Mutation

Adult high-grade gliomas have a large number of genetic abnormalities, including copy number changes and point mutation. Comparatively, pHGG including DIPG have very few mutations, which made it initially unclear what was driving the tumorgenicity of these tumors [15]. In 2012, the fundamental understanding of DIPG changed when researchers discovered the presence of a recurring point mutation that caused histone H3 variants [11, 12]. The most common mutation was a point mutation that converts Lysine 27 to methionine (K27M) in 2 different variants of histone H3: H3.1 and H3.2 [2]. When histones containing this mutation were overexpressed in tissue culture models, the global levels of H3 K27 di- and trimethylation was reduced [16, 17]. The K27 residue on the histone H3 tail can undergo a number of post-translation modification, including acetylation and methylation [18]. The mutation-induced modifications control gene expression levels at specific chromatin loci. Acetylated H3 K27 correlates with increased gene transcription, while H3 K27 trimethylation (H3 K27 me3) silences gene expression. H3 K27 trimethylation is deposited by the enzyme EZH2 which is the part of the Polycomb Repressive Complex 2 (PRC2) [16]. Crystal structures of the H3 K27M histone tail bound to EZH2 revealed that the presence of a hydrophobic methionine in place of lysine on the H3 tail bound to the catalytic domain of EZH2 inhibited EZH2 ability to methylate additional H3 K27 residues [19]. H3 genes have multiple alleles, with H3.1 containing 10 alleles and H3.3 containing 2 alleles, so a heterozygous H3 K27M is considered dominant negative since only one copy needs to be mutated in order to generate the phenotype [20].

PCR2 plays a key role in stem cell differentiation by permanently silencing targeted genes. Embryonic stem cells start will low levels of H3 K27 me3, but as cell fate is restricted, some genes that are not involved in driving cell differentiation are silenced by PCR2 activity [17]. Studies have shown that the presence of H3 K27M prevents silencing of some key embryonic genes involved in cell division and self-renewal. When H3 K27M is removed from DIPG cell models, a decrease in cell growth rate attributed to the silencing of several key genes, such as Olig2 and SOX1, is observed [21, 22]. When expressed at

endogenous levels, H3 K27M does not derepress regions of the chromatin, but rather blocks additional repression sites from forming [23]. Epigenetic signatures of DIPG genomes revealed that the key tumor suppressor gene, CDKN2a, remains silenced by PCR2 despite the presence of the H3 K27M [24]. H3 K27M mutation is specific to pediatric brain tumors in patients between the ages of 6 – 13. Because of the specific conditions in which H3 K27M is tumorigenic, it is hypothesized that rather than resetting differentiated cells, the H3 K27M mutation must occur early enough in development that it can prevent PCR2 mediated silencing and lock in a stem cell like phenotype (Figure 1).

Attempts to model H3 K27Mcontaining tumors in murine models have found that H3 K27M alone is not sufficient to generate tumors in mouse models [25, 26]. Instead, the addition of secondary mutations such as loss of TP53 expression and increased PDGFRA expression is required [25]. The specific variation of histone in which the mutation occurs plays a key role in which secondary mutations are required for tumorigenicity [27]. H3.3 is deposited only in heterochromatin, while H3.1 is deposited in both heterochromatin and euchromatin [28]. The histone deposition pattern is reflected in the epigenetic landscape with H3.1 K27M tumor have markedly reduced trimethylation levels compared to H3.3 tumors [27]. In H3.1 mutated DMG, there is a reoccurring gain of function mutation to the gene ACVR1 which encodes for the receptor ALK2 which is involved in the morphogenetic protein (BMP) signaling pathway [2, 29]. DMG with the H3.3 mutation frequently contain a mutation to either TP53 or PPM1D as well as amplifications of the growth receptor PDGFRa [2]. Murine models have demonstrated that the combination of these specific mutations synergize to increase to rate of glioma like lesions [25].

Although DMG are defined by the presence of H3 K27M mutation, additional driver mutations have been discovered that have inhibitory effects on PRC2 similar to H3 K27M. The histone mutation H3.3 G34R/V is far less common and poorly understand, however recent epigenetic profiles have shown H3 K27 trimethylation patterns similar to H3 K27M mutants [30]. H3 G34R/V mutations have also been implicated in genomic instability through inhibiting DNA repair pathway [31]. Another driver mutation is

a gain of function mutation to the protein EZH inhibitory protein (EZHIP), which has been observed in pHGG and ependymoma [32-35]. The gain of function mutation affects the regulation of PRC2, producing increased inhibition by EZHIP which prevents cell differentiation of specific stemlike genes by PRC2 [33]. In totality, these discoveries have revealed these tumors hijack epigenetic modifications during cell differentiation. Because of this shared characteristic, researchers have targeted epigenetic machinery as a potential therapeutic window for treating DMG.

**1.4 Preclinical Models of DIPG**

Developing preclinical models of DIPG is critical to development and optimization of potential therapies. Accurately modeling all facets of tumor biology in a laboratory setting can be daunting and has led to therapies that show promise in preclinical models but fail in the clinical trials [36]. Most pediatric CNS tumors are removed by surgical resection, which provides samples for murine and tissue culture models. Due to the diffuse nature of DIPG, as well as the sensitive location, these tumors cannot be safely resectioned [1]. Because of this limitation, protocols had to be developed for collecting DIPG tissue during patient autopsies. The tumor is removed during the autopsy 2-4 h after patient death [37]. Tissue collected was initially cultured in standard tissue culture conditions with DMEM media. DIPG cells could be grown as either neurospheres or a monolayer [38]. Strategies for optimizing growth of DIPG in tissue culture have included immortalizing cells with hTERT modifications and using neural stem cell media as well plates coated in laminin-b [38]. DIPG tissue from autopsies can also be used to generate murine models by injecting cells into the pons of immunodeficient mice. These xenografts can be directly injected or cultured prior to injection. Monje et al reported that direct injection induced the formation of murine CNS tumors, while indirect injection after cell culture did not induce murine tumors [39].

The development of these models allowed for a testing of novel targeted therapies. Tissue culture models offered a higher throughput method of testing chemical agents but lacked the tumor

microenvironment and pharmacokinetic/dynamic effects that are present in xenograft models [40]. Monje's team screened a large library of small molecule inhibitors on DIPG tissue culture lines and identified HDAC inhibitors such as Panobinostat as a potent therapy of DIPG with the histone mutation [41]. Although using autopsy lines as a pre-clinical model have provided a wealth of knowledge, some of the targets identified have not translated when tested in clinical trials [40]. Panobinostat showed promise in multiple preclinical models but did not show efficacy in DMG patients at the maximally tolerated dose. It is unclear at this point whether the lack of efficacy in human trials was due to poor blood brain barrier penetration or another reason [36].

While there are many reasons why cancer drugs fail to translate from preclinical studies to human clinical trials, DMG translational studies stood out as the single instance in which all models were derived from autopsies of pediatric DMG patients. One of the challenges with autopsy-derived models is that the cells have already been exposed to treatment such as radiation and chemotherapy. Undergoing radio and chemotherapy can have a profound impact on tumor biology by inducing additional mutations and driving clonal selection of more resistant tumor populations [42].

Another strategy for modeling DIPG is the use of genetically engineered mouse models (GEMM). The advantage of GEMM models is that they can recapitulate some of special and temporal aspects of tumor development in humans. The earliest technique for generating GEMM models involved the use of the avian sarcoma leucosis virus (RCAS) vector [43]. In the RCAS system, mice are genetically altered as pups to express the tumor virus A (TVA), which allows for tissue specific infection of TVA expressing cells. Becher et al expressed TVA under a pons specific nestin promoter and infected the pons with RCAS vector for DIPG hall mark mutations [44]. The first RCAS model had genetic alterations to H3.3 K27M, PDGF-B and p53. Mice that received these alterations developed high grade gliomas in the brainstem and showed a reduction of H3 K27me3, demonstrating recapitulation of this key characteristic of DIPG. Additional RCAS models have been generated for H3.1 K27M, ACHR1 R206H subtype [45]. RCAS models have

provided a platform to retest targeted therapy, with the most notable example being histone demethylase inhibitor GSKJ4, which was shown to remove K27me3 at the CDKN2a loci and induce senescence in RCAS models [46]. An alternative GEMM strategy has been the use of human embryonic stem cells to seed tumors in the pons of mice. Human embryonic stem cells can be modified to contain H3 K27M along with additional secondary mutations [26]. These models have been crucial for understanding the pathophysiology of the H3 K27M mutation, but it is unclear if GEMM models accurately recapitulate the epigenetic landscape, tumor heterogeneity, and tumor microenvironment observed in DIPG patients.

A more recent advance in DIPG preclinical models has been the success of stereotactic biopsies in patients prior to treatment [47-49]. Multiple institutions, including Seattle Children's Hospital, have set up cross-disciplinary platforms for collecting treatment naive biopsies of DIPG. The protocol for collection brainstem biopsies using MRI imaging and CT scans is to identify tumors while avoiding necrotic tissue and blood vessels. Stereotactic robots coordinate with the imaging data to remove a biopsy core, which can be cultured or used to implant xenografts. Treatment naive biopsies have advantages over autopsy lines in that they are more representative of how the tumor will respond to treatment [48]. Werbrouck et al measured the radiation sensitivity of biopsy lines and found they directly correlated with how that patient responded to radiation therapy in the clinical setting [50]. The advance of treatment naive biopsy lines for DIPG may finally provide pre-clinical models that will enable successful translation of translational research findings to clinical therapies.

**1.5 Radiation Therapy in DMG**

**Radiation therapy:**

Radiation therapy has been used as a therapy to manage tumors for over a hundred years. The most common form of radiotherapy is photon radiotherapy, which utilizes ionizing radiation to damage the nucleic acids of tumor cells [51]. Radiation therapy is optimal for treating brain tumors because it is

noninvasive and not limited by BBB penetration the way chemotherapy is. With new technology such as image guided radiation therapy and 3d conformal treatment allowing for precision targeting, radiation therapy can now directly target the tumor mass with limited radiation dosage to healthy tissue [52]. Radiation is measured in grays (Gy), which is defined as the amount of energy absorbed per mass (J/kg). The standard method for radiation administration in DIPG patients is fractionated, dosing at 2 Gy per day up to a total of 60 Gy over the span of several months [53]. Patients will typically receive steroids to manage adverse symptoms caused by radiation-induced swelling in addition to the bulk of the tumor mass within the confines of the skull [53]. Although radiation therapy can transiently stabilize the disease, tumor recurrence is inventible in DIPG patients. The median overall survival for patients following radiation therapy is still in the range of months [54]. This is a stark contrast to most other pediatric tumors of the CNS, which are generally radiation sensitive [1]. There is something intrinsic to the biology to DIPG that allows it to rapidly recover from a radiation event.

**DNA Damage Response:**

The primary way in which radiation damages cells is through is through the ionization of genomic DNA. Photon beams generate reactive oxygen species, which attack DNA phosphate backbone and induces single strand nicks in the DNA strands [55]. If these nicks occur in close proximity on the genome or are not repaired in a timely manner, they will induce double strand break (DSB), which is more difficult for cells to repair and leads to more adverse effects [56]. Cells use a complex set of signal transduction pathways to assess DNA damage and carry out the appropriate cellular response; these pathways cumulatively are known as the DNA damage response (DDR) [57, 58]. DDR is initiated following DNA damage protein kinases ATM and ATR, which trigger a phosphorylation cascade that coordinates DNA repair. Upon activation, ATM phosphorylates serine 139 on histone H2AX at the site of DSB. Phospho-H2AX recruit DNA repair proteins such DNA-PKcs and Ku70//80. If cells are in S or G2 phase, they can undergo homologous repair (HR) in which a sister chromosome is used as a template to repair DSB without

the addition of extra mutations [56]. If the cells do not have access to HR, they will undergo non-homologous end joining (NHEJ) [59]. NHEJ can occur during any phase of the cell cycle, however it is error-prone and induces additional mutations. ATM and ATR activate downstream checkpoint kinases CHK1/CHK2 as well, which coordinate the proper cellular response [60-62] (Figure 2). Depending on the severity of the DNA damage, cells may undergo growth arrest or cell death via apoptosis. Key proteins in growth arrest are CHK1 and WEE1 which block key the cell cycle at checkpoints if the genome is too unstable for cell division [56]. TP53 rapidly accumulate during DDR and begins transcribing pro-apoptotic proteins such as NOXA and PUMA [63, 64]. These proteins inhibit the pro-survival BCL family proteins that sequester the effector proteins BAX and BAK. Upon release from sequestration, BAX and BAK dimerize on the mitochondrial membrane generating pores that release cytochrome c from the mitochondria. Once cytochrome c is released, the cell will undergo controlled cell death via the apoptosome [65].

Tumors have developed several strategies to redirect the DDR in order to resist DNA damaging therapies such as radiation [66]. Radiation is typically more effective in rapidly cycling cells such as tumors because these cells are more frequently in S phase [67]. In S phase, cells unwind DNA at a replication fork and generate single strand DNA to be used to generate the daughter DNA. SSB during this replication fork generate DSB in the daughter DNA, which causes tumor cells to undergo more DNA damage compared to normal tissue [67]. To resist DDR, tumors have employed multiple strategies including upregulating DNA repair and redirecting cell fate away from senescence and apoptosis. DIPG cells typically contain mutations in genes that encode key members of the DDR, such as p53 and CDKN2a [2]. These mutations cripple the signal transduction process and protect against apoptosis and senescence. DIPG have also been shown to upregulate WEE1 which safeguards from mitotic catastrophe in which a cell undergoes mitosis because of too much DNA damage [68, 69]. Controlling cell fate is also a mechanism by which tumors avoid cell death. By over expressing pro survival factors such as BCL-2, tumors can avoid apoptosis and only undergo cell cycle arrest. BCL-2 inhibitors such as navitoclax have been developed to overcome

overexpression of BCL-2 proteins [70]. Considering the resistance of DIPG to radiation therapy compared to other pediatric brain tumors, there may yet be additional mechanisms by which these cells can overcome DNA damage and DDR.

**Combination Therapy with Radiation**

Since radiation is the only therapy to show a modest improvement to overall survival, there has been an effort to improve radiation efficacy with radiosensitizers [53]. Radiosensitizers typically target DNA repair mechanisms and attempt to overcome the mechanisms tumors use to resist radiation. It is common for oncologists to add chemotherapy, such as temozolomide and etoposide, in combination with radiation therapy [71]. These agents increase DNA damage sustained by cells but play no role in the DNA repair or DDR. To date, no congruent chemotherapy agents have provided significant improvement to patient survival. More targeted approaches have been developed in pre-clinical models to attempt to overcome radiation resistance mechanisms in DIPG. Some DIPG have been shown overexpress PARP1 which is involved in repair of SSB [72, 73]. PARP inhibitors have shown to have some anti-tumor efficacy when paired with radiation in xenograft models, however it is unclear how well these models translate since the xenografts were high-grade astrocytoma rather than DIPG lines [73]. WEE1 is another target that is over-expressed in some DIPG patients and is hypothesized to protect DIPG cells from radiation therapy [69]. WEE1 inhibitors have shown radio-sensitizing capabilities in tissue culture and xenograft models with DIPG autopsy lines. There is currently a phase 1 clinical trial to assess the efficacy and maximum tolerated dose of the WEE1 inhibitor adavosertib (MK1775) [74]. The challenge with targeting DNA repair mechanisms is that it may sensitize normal tissue to radiation as well, leading to severe toxicity.

To exploit the altered genetic landscape in DIPG compared to normal tissue, some investigators have evaluated epigenetic modulators as radiosensitizers. Histone demethylase inhibitors such as GSK-J4 help overcome the H3 K27M inhibition of PRC1 and increase global levels of H3 K27me3 [46]. These drugs

have been shown to be potent radiosensitizers in autopsy lines as well as RCAS models, suggesting the epigenetic state of DIPG may have some protective role in radiation resistance. Another epigenetic modifier that is targeted is BMI-1, which is a member of the polycomb repressive complex 1 (PRC1). BMI-1 is responsible for inducing HR and is highly upregulated in DIPG due to dysregulation caused by H3 K27M [75, 76]. The BMI-1 inhibitor PTC596 is currently in phase 1b clinical trial. Despite the widespread pre-clinical success of radiation sensitizers, none of these treatments have translated to improvements in the clinic. The primary pre-clinical model for radio-sensitizing drugs have been autopsy-derived lines, which are derived from tumors that have previously been heavily treated with radiation. These lines may have limited utility compared to treatment naive biopsy lines in studies that focus on developing therapies for DIPG patients at the time of initial diagnosis. Recently the Castel lab measured radiation resistance in treatment-naive biopsy lines and discovered that the cell line's susceptibility to radiation directly correlated with how patients performed in clinic [50]. They went on to screen these lines using a CRISPR library for protein kinases and identified ATM and CHK1 as key proteins for resistance to radiation. Although these studies are still in their early stages, treatment-naive biopsy lines of DIPG may help overcome the gap between efficacy in pre-clinical models and efficacy in clinical trials.

**1.6 Figures:**

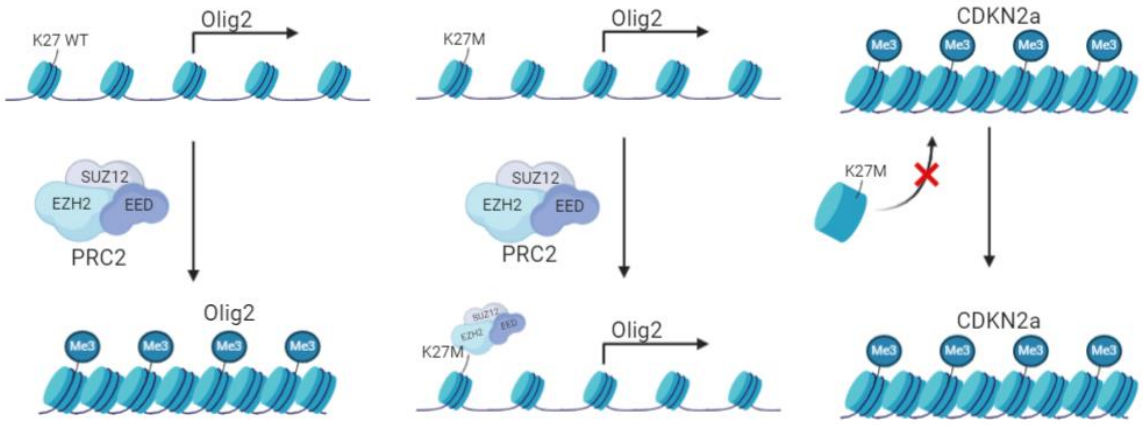


**Figure 1 Legend: Schematic of H3 K27M Oncogenesis:** H3 WT allows propagation of K27me3 by PRC2 during cell development. The presence of K27M binds to EZH2 in the PRC2 and blocks K27me3 propagation and maintain expression of stem like genes. Regions of chromatin that are already repressed do not accumulate the K27M mutant and remain repressed.

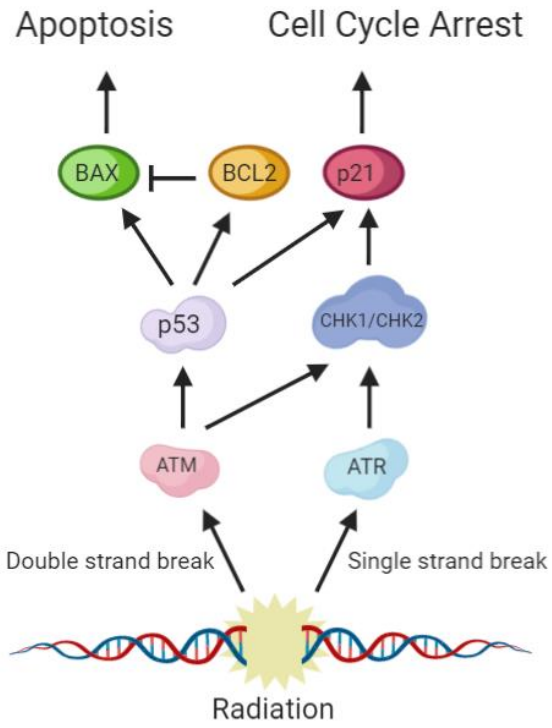


**Figure 2 Legend: Schematic of DNA Damage Response:** Radiation induces DNA damage which can lead to cell cycle arrest or apoptosis.

## Chapter 2 Radiation Sensitivity in Treatment-naïve Biopsy Derived DIPG Models

### 2.1 Abstract:

Therapies developed in pre-clinical models of DIPG have failed to show any significant improvement on patient survival. The most frequently used pre-clinical models involve DIPG lines generated from autopsies. Because autopsy samples have invariably undergone radiation the chemotherapy, these models are not representative of treatment-naive tumors. Treatment naive tissue is difficult to obtain because DIPG cannot be safely removed by surgery. We have developed a method to remove biopsies safely using a stereotactic removal. These biopsies were then used to develop tissue culture lines as well as xenograft models. Cells acquired from treatment naive tumors demonstrated resistance to radiation that correlated with clinical responses to radiation. We investigated if the presence of the mutant histone was driving radiation resistance though DNA repair and found no link between the presence of the H3 K27M and DNA repair rates.

### 2.2 Introduction

DIPG is an aggressive pediatric brain tumor which arise in the midline structures of the CNS. In patients with DIPG, the average overall survival is 12 months with a 5-year survival rate of less than 1% [1, 14]. Current standard of care involves focal radiation given in daily 2 Gy fractions up to 54 Gy, however this only improves life expectancy by around 3 months [53]. Chemotherapy such as temozolomide and etoposide are utilized, however, only radiation therapy has shown a significant improvement in patient survival [71, 77]. Because these tumors cannot be resected, there have been limited tissue samples to use as pre-clinical models in order to develop new therapies [48]. Researchers have focused on DIPG lines derived during autopsies; however, research has shown that DIPG undergo molecular changes following radiation and chemotherapy. Hoffman et al looked at tumor heterogeneity in patient autopsies and found that while all cells contained conical mutations to H3 K27M and TP53, clonal populations contained

additional mutations to PIK3CA and FGFR1 among others [42]. This study suggested that there are temporal and spatial changes that occur during tumor progression. Prolonged expansion of tumor lines in tissue culture can also be problematic since cells will adapt to growth conditions and may lose some of its original biology. In order to accurately assess the therapeutic window of treatment on primary tumors, we developed a protocol to collect primary tumor biopsies with minimal health concerns for patients. In order to obtain a core biopsy, patients or the primary caregiver consent to the surgical procedure and donation of tissue sample for research purposes. While early biopsy does not affect standard initial therapy of 54 Gy focal radiation, it provides opportunities to evaluate mutations that may be targetable.

## 2.3 Results

### Treatment naive DIPG model development from biopsy derived tissue

DIPG is considered to have a classic imaging appearance by MRI, however there are some inconsistencies in imaging interpretations. With MRI, DIPG are visualized having a diffuse hyperintensity throughout the majority of the pons, which is typically evident at the time of diagnosis (figure 1A-D). Using MRI preoperative imaging, the neurosurgeons on our team determine the best biopsy location, typically closest to the lateral posterior edge of the tumor. Once the patient is intubated and positioned prone in rigid, Mayfield fixation, the surgeons generate a burr hole via the posterior fossa. If this procedure is deemed safe during the procedure, the surgeons attempt to collect 8 core specimens at 2 different depths along the trajectory. The risk of adverse events such as hemorrhaging, cranial nerve palsies and focal neurological deficits is low, but is still monitored for safety concerns.

Two cores are fixed and used for routine histologic and molecular profiling. The top priority is to use samples for diagnostic approaches with a secondary goal of providing tissue for research. Following histologic diagnosis, samples are submitted to Laboratory Medicine at the University of Washington, where DNA is extracted and used for targeted gene sequencing via UW-oncoplex. Genes sequenced

include those that are frequently mutated in pHGG including: H3F3A (H3.3), HIST1H3C (H3.1), TP53 and EGFR. The remaining core samples are used to establish pre-clinical models or frozen for future genomic studies.

Specimens are received on ice within 4 hours of surgical acquisition. A typical biopsy contains enough tissue to initiate tissue culture and implant orthotopic xenografts in immunodeficient mice. The tissue sample is carefully transferred to a small volume of Neurocult Complete (NC) media where a sample is split in two by mechanical manipulation. Samples for establishing xenograpfts are stored on ice and implanted in immunodeficient mice as described previously __. The remaining mass is dissociated into single cells before being transferred to a T25 flask containing 10 mL of Neurocult (NC) and grown for several days at 37˚C in 5% $CO_2$. The culture initially contains additional human cells including macrophages, red blood cells and normal brain tissue, however after several passages the cultures become homogenous for tumor cells. After the tumor has stabilized in the flask, cells are transferred to a flask containing Laminin b derived from Engelberth-Holm-Swarm sarcoma tumor basement membranes. While not all DIPG lines require laminin, it has been critical for sustained growth of the majority DIPG biopsy lines. To date, we have generated orthotopic xenograft mouse models or cell lines from five treatment-naive DIPG biopsies. All lines showed histological features of high-grade glioma (Fig. 1E-H) Analyzing the UW-Oncoplex sequencing data, has revealed a number of the key molecular mutations that are hallmarks of DIPG. The five cell lines generated are listed in Fig. 1.

**Radiation Sensitivity of Treatment Naive DIPG cell lines**

Using these treatment naive lines, we sought to determine if their response to therapy matched the patients from which they were generated. Clonogenic assays are the standard for assessing cellular response to radiation. We found however that the treatment-naive lines were not amenable to clonogenic

assays since the cells required direct contact with other cells in order to maintain consistent growth. Single cells were unable to develop clonal populations under tissue culture growth conditions. To overcome this, we developed a method to assess radiation in monolayer tissue culture in response to a range of radiation doses (Fig. 2A). We plated cells in a 96 well plate and treated each cell with ionizing radiation generated from an X-Rad 360 . Radiation was generated in a 2D field, which allowed us to control the radiation dose in each well. Cell viability was measured via cell titer glo after incubating cells for 72 h post radiation. We used 8 doses of radiation in order to generate dose response plots, with three technical replicates for each radiation dose. Using the dose response curves, we calculated the $IC_{50}$ and the maximum response for each DIPG line. We compared dose response curves of DIPG lines to medulloblastoma lines which were also treatment-naive and derived from surgical resections. Medulloblastoma is a pediatric brain tumor that responds more favorably to radiation therapy in clinical practice compared to DIPG, which typically exhibits limited or no decrease in tumor mass following radiation therapy.

To correlate radiation-resistance in our patients and their corresponding cell cultures, we reviewed each patient's progression-free survival and overall survival. Two cultures (PBT-22FH, PBT-24FH) were generated from patients who experienced early progression despite standard ~54 Gy focal radiation: the former progressed at day 121 and died on day 190 post-diagnosis, while the latter progressed 79 days post-diagnosis and died on day 222 post-diagnosis. In contrast, the patient represented by PBT-09FH, did not experience progression until 284 days post-diagnosis, and death occurred on day 468. The patient from whom PBT-27FH was derived experienced tumor progression on day 288 and remains alive. To assess the cultures' radiation-resistance, we treated them with 0-45 Gy and measured cell viability at 96 hours (Fig. 2a). PBT-22FH and PBT-24FH showed 69.1% and 78.1% viability, respectively, after 32 Gy (Fig. 2a). In contrast, PBT-09FH had only 32.6% viability under the same conditions. These data support the previous observation that radiation resistance in DIPG models is predictive of how patients will respond in the clinic (reference needed).

The dose response curves were compared to autopsy-derived lines that were obtained from the Monje lab as well as treatment-naive medulloblastoma lines obtained from surgical resections in newly diagnosed patients. In order to compare dose response curves among groups, we used a non-linear regression analysis with three parameters to calculate $IC_{50}$ and maximal dose response, which was defined as the bottom plateau of the dose response curve. Both the treatment-naive and autopsy-derived DIPG lines exhibited a wide range in radiation $IC_{50}$ (Fig. 2b). Using one-way ANOVA analysis with Dunnett's multiple comparison analysis, we determined that there was no significant difference between $IC_{50}$ in treatment-naive vs. autopsy lines ($p > 0.05$), however the $IC_{50}$ in both lines was significantly higher than the pretreatment medulloblastoma lines ($p < 0.05$). This is in line with clinical observations in which DIPG show limited growth reduction from radiation while medulloblastoma patients see a marked reduction and a much longer delay before tumor recurrence. Interestingly the maximum response plateau was significantly higher in the treatment-naive biopsy lines compared to the autopsy lines by one-way ANOVA analysis with Dunnett's multiple comparison analysis ($p < 0.05$). Multiple variables may contribute to how low maximum response is including cell growth rate and the ratio of growth arrest to cell death. While we cannot conclude what mechanism accounts for this difference, it demonstrates the biological differences between these lines. Every DIPG measured plateaued above 0% which was a stark contrast to the medulloblastoma lines which were completely eradicated at higher doses. We did a preliminary experiment in which we measured the fold change in apoptotic cells following radiation using the apoptotic marker Annexin V. We saw minimal fold increase in DIPG lines while the medulloblastoma had a threefold increase in apoptotic cells. Based on this data we hypothesized that the radiation resistance observed in DIPG is directly rated to the low rate of apoptosis following radiation therapy.

**H3 K27M Effect on DNA Repair Kinetics**

Since we observed a discrepancy in the radiation response between DIPG compared to radiosensitive tumors, we wanted to test if the H3 K27M was driving the discrepancy. One potential

mechanism by which H3 K27M may affect the DDR is by effecting DNA repair kinetics. Histone modifications help coordinate DNA repair by several mechanisms [78]. First histone H2AX is phosphorylated by ATM at the site of DNA damage [79]. Next histone acetyl transferases (HAT) acetylate the H3 tail allowing for the chromatin to be opened so repair proteins can access the DNA [80]. Since DIPG with H3 K27M typically have more open chromatin due to the repression of PRC2 activity, we hypothesized that DNA repair is faster in DIPG.

To test this hypothesis, we used a neuro stem cell (NSC) CB660 which contained wildtype histones. We used a Tet on system that expressed either H3 WT, H3 K27M or H3 G34R. These histones were flag tags to allow for quantification by western blot. Using different concentrations of doxycycline, we were able to induce histone expression at endogenous levels (Figure 3A). We confirmed that histones were incorporated into the genome by staining for flag in combination with DAPI (Figure 3B). In order to measure response to radiation, we measured gamma-H2AX (phosphor Ser 139) foci at a set time point post radiation. This has been previously shown to be a quantifiable method for assessing DNA repair rate. We compared the gamma H2AX foci one-hour post 1 Gy of radiation in H3 K27M and H3 G34R compared to H3 WT (Figure 3D). We compared each group by two tailed unpaired students T-test between WT histone compared to either mutant. We found no significant different in K27M but saw increased DNA damage in cells containing H3 G34R. G34R has been reported to drive genome instability so this is inline with the current research [31]. Interestingly we did not observe a reduction in H3 K27me3 when expression K27M at endogenous levels. Other research groups have looked into DNA repair in H3 K27M and found no significant difference in DNA repair rate. We concluded from these experiments that the resistance to apoptotic pathways must occur at the DDR signaling pathways and not at the level of DNA repair.

**2.4 Discussion**

We have developed a safe and viable protocol for collecting treatment-naive biopsies of DIPG that we can be used to establish non-clinical models. These tumor cells are amenable for both tissue culture and xenograft model generation. The conditions required for tissue culture or xenograft growth vary markedly from patient to patient. Some lines such a PBT-09FH grow well as xenografts but grow poorly in tissue culture. As we continue to optimize growth conditions, we will increase our repertoire of non-clinical models. Other groups around the world have also set up platforms by which to collect DIPG biopsies and the hope is that it will be the gold standard for pre-clinical models going forward. Using these models, we have demonstrated these models are somewhat correlative of how DIPG tumors respond in clinic. This result is also supported by a previous study conducted by the Castel lab. They also reported specific mutations, including TP53 mutations, that correlated with particularly poor radiation responses in the clinical setting. One potential use for biopsy lines going forward is to help predict which therapies will be effective for that specific patient. For tumors which are highly resistant to radiation, it may indicate that the patient should either avoid radiation or receive a radio-sensitizing agent in combination.

We wanted to see if the H3 K27M mutation was responsible for the discrepancy we saw in radiation response between DIPG and other pediatric brain tumors. Among DIPG, H3 mutant lines have a significantly worse survival compared to histone wild type tumors. We tested if this mutation played a role in DNA damage response and found no significant difference between cells expressing H3 K27M and cells expressing H3 WT. Other research groups have looked into this as well and found no link between the mutation and DNA repair. Based on these results we decided to focus more on the proteins involved in the apoptosis pathway. We focused specifically on genes that are dysregulated in DIPG and how they may drive cell fate away from apoptosis following radiation.

## 2.5 Methods

### Histology

Paraffin section were cut and placed on charged slides. Hematoxylin and Eosin (H&E) staining was performed in the standard fashion. Immunohistochemical staining was performed using a Ventana Benchmark Stainer (AZ, USA). Sections were incubated with primary antibody to H3 K27M at 1:1200 (Millipore; CA, USA). Slides were incubated with biotinylated secondary antibodies, followed by incubation with the streptavidin and biotinylated peroxidase complex. Sections were counterstained with hematoxylin and mounted.

### Human specimen and patient-derived cell cultures

Human cell cultures were generated with informed consent in compliance with Institutional Review Board (IRB) approval at Seattle Children's Hospital (#14449), Children's National Medical Center (#1339), and University Children's Hospital Zurich (#2019-00615). PBT-09FH, PBT-22FH, PBT-24FH, PBT-27FH, and DRIz-D105 were biopsy-derived at diagnosis. For PBT-09FH, PBT-22FH, PBT-24FH, PBT-27FH, and MED-411 tumor tissue was obtained at Seattle Children's Hospital and cell cultures were created at Fred Hutchinson Cancer Research Center (FHCRC). HSJD-DIPG007, from Dr. Angel Montero Carcaboso (Hospital Sant Joan de Deu, Barcelona, ESP), and SU-DIPG48, from Dr. Michelle Monje (Stanford University, Stanford, CA, USA), were generously donated to University Children's Hospital Zurich. Cells were maintained in NeuroCult NS-A Basal Medium with NS-A Proliferation Supplement (STEMCELL Technologies; Vancouver, CAN), 1X Antibiotic/Antimycotic (ThermoFisher Scientific; MA, USA), 40 ng/mL epidermal growth factor (PeproTech; NJ, USA), and 40 ng/mL fibroblast growth factor (PeproTech; NJ, USA). All cell culture models were validated by DNA fingerprinting.

**Drugs, radiation, cell viability assays, apoptosis assays**

Radiation studies were performed using an X-rad 320 Precision X-ray (Precision X-Ray, Inc.; CT, USA) using stage position 4, 320 KV, and 12.50 mA on filter 1. For cell viability studies following radiation, 96-well plates were coated in 10 µg/mL of laminin (Sigma-Aldrich; MO, USA) in DPBS and incubated for > 4 hours, after which 15,000 cells per well of a single-cell suspension were plated, 24 hours later irradiated, then viability was measured 96 hours later. Cell viability was measured using CellTiter-Glo® Luminescent Cell Viability Assay (Promega; WI, USA), and data was collected on a Synergy 2 plate reader (Bio-Tek; VT, USA). Flow cytometry was performed on a NovoCyte Flow Cytometer (ACEA Biosciences; CA, USA) using Annexin V-FITC (Biolegend; CA, USA) and data was analyzed using FlowJo software (Becton-Dickinson; NJ, USA). Cell viability for CNMC-XD-760, DRIz-D105, CNMC-D967, CNMC-D1008, HSJD-DIPG007, and SU-DIPG48 cell, was done by plating 5,000 cells/well into 96-well plates, then, after 24 hours, cells were exposed to drug for 72 hours. Viability was measured by using CellTiter-Glo™ assay (Promega; WI, USA) and data were collected on a Biotek Cytation 3 luminescence reader.

**Tet on construct and Immunofluorescence**

H3 K27M, H3 WT and H3 G34R obtained from Henikoff lab in pcDNA4 backbone. H3 gene was transferred to pEN_TTmcs (addgene) with tet on promoter. Gateway cloning was used to put tet on system in lent backbone pENTT (addgene). pENTT was transfected (lipofectamine 2000) with lenti packaging and envelope vectors in HEK293 and media was collected after 24 h. CB660 infected at MOI 0.3 under puro selection. Antibodies used were β-Tubulin (ab189511) Mouse mAb at 1:5000 (abcam), γ-H2A.X (phosphor S139) Rabbit mAb (EP8542Y) at 1:100 in IF (abcam). Cells fix for IF with methanol and stained with DAPI and γ-H2A.X overnight at 4 C. Imaging done on Deltavision wide field miscroscope.

## 2.6 Figures

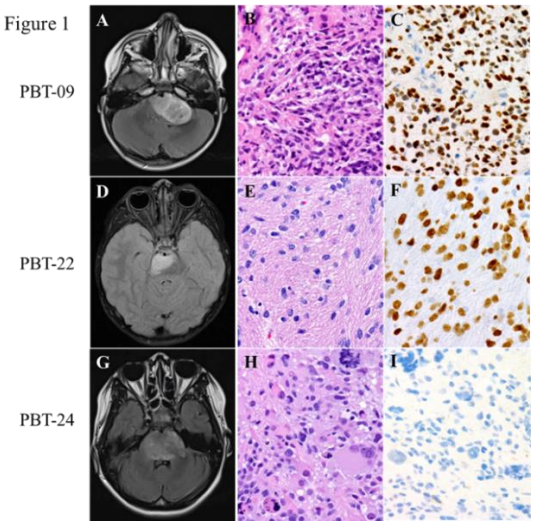


| Tumor lines: | Mutations | Tissue culture | Xenograft |
|---|---|---|---|
| PBT-09FH | H3.3 K27M | No | Yes |
| PBT-22FH | H3.3 K27M | Yes | No |
| PBT-24FH | H3 WT HGG | Yes | Yes |
| PBT-27FH | H3.1 K27M | Yes | No |
| PBT-29FH | H3.3 K27M | Yes | Yes |

**Figure 1 Legend: Histology and MRI Images for DIPG Biopsy Samples. (A)** MRI Brain Axial T2 FLAIR with contrast, **(B)** H&E immunohistochemistry (IHC), and **(C)** positive H3 K27M IHC. Clinical correlates for patient providing PBT-22FH including **(D)** MRI Brain Axial T2 FLAIR, **(E)** H&E IHC, and **(F)** positive H3 K27M IHC. Clinical correlates for patient providing PBT-24FH including **(G)** MRI Brain Axial T2 FLAIR with contrast, **(E)** H&E IHC, and **(F)** negative H3 K27M IHC.

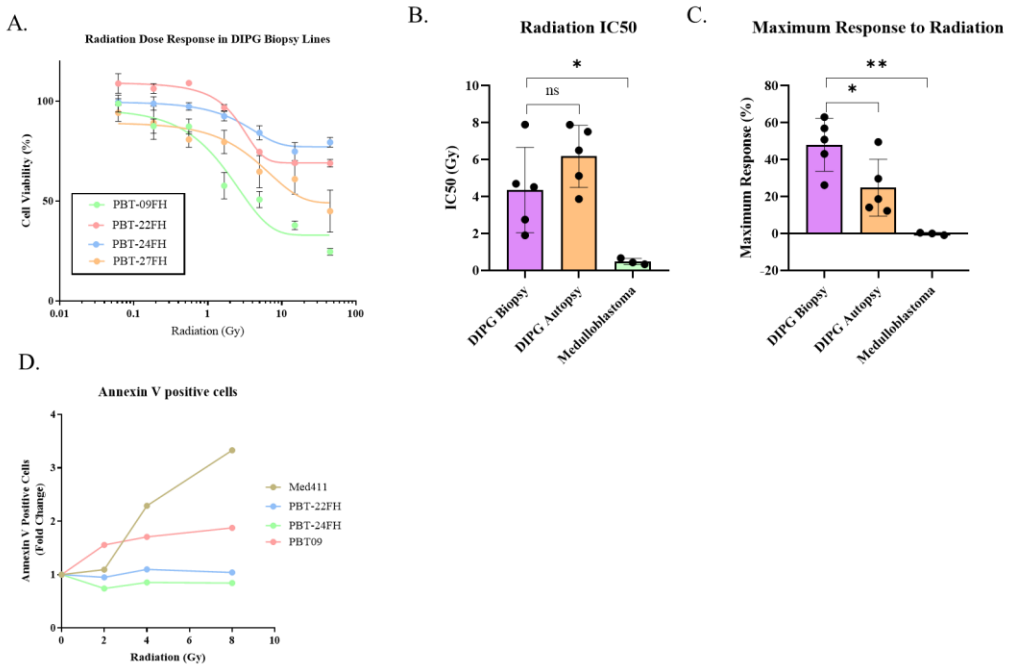


**Figure 2 Legend: Radiation Dose Response in Treatment Naive DIPG Lines. (A)** Radiation dose response curves of treatment naive DIPG biopsy lines. **(B)** Radiation $IC_{50}$ calculated by non-linear three variable curve for DIPG biopsy, autopsy and medulloblastoma lines. **(C)** Maximum response calculated as the bottom plateau of nonlinear fit model.

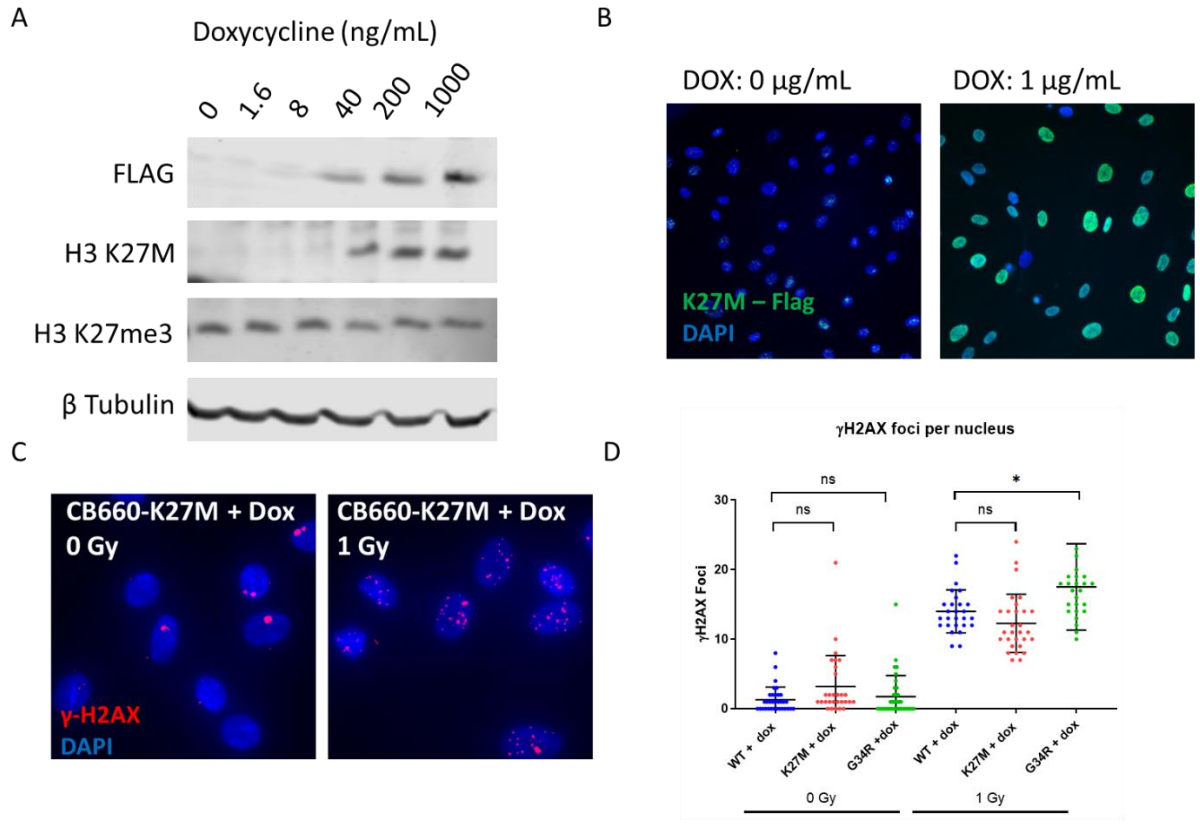


**Figure 3 Legend: Role Histone Mutations Play on DNA Repair Rates. (A)** Western blot of Tet on system showing expression of flag tagged H3 K27M at increasing levels of doxycycline in NSC line CB660. **(B)** IF of CB660 for Flag tag and DAPI +/- doxycycline. **(C)** γ-H2AX staining conducted 1 h post radiation. Cells incubated with doxycycline at 1 µg/mL 48 h prior to radiation. **(D)** Quantification of γ-H2AX per nuclei in each histone variant. Statistics calculated as two tailed unpaired Student T-test to H3 WT.

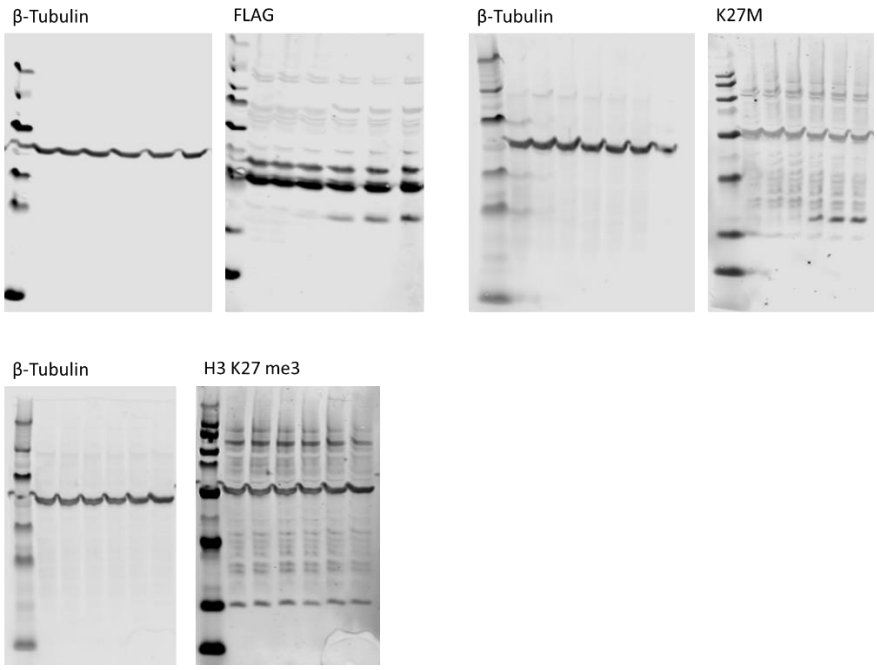


**Supplementary Figure 1 Legend: Raw Western Blot for Figure 3. (A)** CB660 with H3 K27M flag tag for anti-FLAG **(B)** CB660 with H3 K27M flag tag for anti-H3 K27M **(C)** CB660 with H3 K27M flag tag for anti-H3 K27 me3

## Chapter 3: Reduced BAX Expression Drives Resistance to Radiation Induced Apoptosis

### 3.1 Abstract:

Radiation is the only treatment so show a significant benefit to patient overall survival and symptom free survival in DIPG. This benefit only improves life expectancy by several months. There is need to identify the mechanisms by which DIPG resists radiation and discover target therapies that improve the efficacy of radiation. We previously observed that DIPG lines have much lower rates of apoptosis following radiation compared to other pediatric brain tumors. We report that the pro-apoptotic protein BAX is expressed in lower basal levels in DIPG and is not upregulated following radiation. In order to overcome the decrease in pro-apoptotic inhibitors, we suppressed the anti-apoptotic BCL family members with Navitoclax. DIPG lines showed higher rates of apoptosis with the combination therapy compared to radiation alone. Because Navitoclax fails to cross the blood brain barrier, we tested its ability to enhance the effects of radiation in flank models of DIPG to establish proof-of-concept. Mice treated with the combination therapy survived, on average days longer than those treated with radiation alone, suggesting that a blood brain barrier penetrating BCL inhibitor could potentially be assessed in clinical trials to improve radiation efficacy for DIPG patients.

### 3.2 Introduction:

Diffuse midline gliomas (DMG), which includes Diffuse Intrinsic Pontine Gliomas (DIPG), is a class of pediatric high-grade gliomas characterized by unique molecular features and an extremely poor overall prognosis [2]. Due to the diffuse infiltration of these tumors throughout the brainstem, surgical resection is not an option [47]. Radiation is the only therapy to show a transient response in DIPG, while chemotherapy has not extended patient survival [81-83]. Because of the aggressive nature of DIPG coupled with treatment challenges, the 5-year survival for patients with DIPG is <1% [2]. The low survival

rate has made it imperative that researchers understand the molecular mechanisms that underlie treatment resistance in order to improve the poor prognosis in DIPG patients.

A common feature of DIPG is a reoccurring mutation to Histone H3 variants. The most frequent mutation, occurring in around 85% of DIPG, involves the conversation of Lysine 27 in either H3.1 or H3.3 to a methionine (H3K27M) [12, 84]. H3 histones containing the K27M mutations have an antagonistic effect on the Polycomb Repressive complex PRC2 complex which is responsible for the propagation of the H3 K27 trimethylation mark [85]. H3 K27 trimethylation is predominantly used to repress specific regions of chromatin during cell differentiation [86]. The inhibition of PCR2 by K27M is thought to prevent differentiation of glial stem cells and prime them to become tumorigenic with the addition of secondary mutations such as TP53 loss or PDGFRA amplification. Other DIPG mutations, such as those involving H3.3 G23R/V and EZHIP have been shown to similarly inhibit PCR2, leading to tumors that are phenotypically similar to those driven by H3 K27M [32]. This unique epigenetic landscape and stem cell phenotype of DIPG drive the aggressive nature of these tumors but may also offer a unique therapeutic opportunity for targeting these tumors.

Because radiation therapy (RT) extends life expectancy by an average of 8-9 months, a number of DIPG research efforts have focused on optimizing radiation [46, 50, 82, 83]. DIPG tumors differ from other frequently occurring pediatric brain tumors in that there is little to no reduction of tumor mass following radiation. DIPG tumors will typically have a lag phase of growth arrest before relapsing after around 5 months. We set out to understand whether, in contrast to radiation-sensitive pediatric brain tumors such as some types of medulloblastoma, DIPGs fail to undergo apoptosis following radiation-induced DNA damage and to understand the molecular mechanism if so. Ionizing radiation induces apoptosis by damaging DNA leading to a DNA damage response. TP53 and CHK1/CHK2 pathways initiate both pro survival and pro-apoptotic pathways depending on the magnitude of damage. The pro-apoptotic proteins BAX and BAK are activated and dimerize to form pores at the mitochondrial membrane. This releases

cytochrome c and drives the apoptosis process. Pro survival proteins like BCL-2 family proteins bind directly to BAX and block this dimerization. The ratio of the pro survival and pro-apoptotic proteins determines a cell's response to ionizing radiation.

The following studies were prompted in part by our observation that BAX mRNA levels were diminished in some DIPG patients, potentially leading to an imbalance between BAX and anti-apoptotic counterparts. We further showed that BAX levels do not increase in our DIPG models in response to radiation, in contrast to radiation-sensitive pediatric brain tumors. Because BAX levels were low, but not absent in DIPG, we hypothesize that the combination of BCL-2 inhibitors with radiation in DIPG will induce radiation-triggered apoptosis in DIPG and improve treatment efficacy. To test our hypothesis, we screened BCL-2 family inhibitors and identified a candidate that synergized with radiation to induce extensive apoptosis in DIPG but not neural stem cells (NSC).

### 3.3 Results

#### BAX Protein is Significantly Reduced in DIPG Compared to Other Pediatric Brain Tumors

We and others previously showed that DIPG cells fail to undergo apoptosis in response to radiation. Using gene mRNA levels obtained from the public data base Children's Brain Tumor Tissue Consortium (CBTTC), we determined that the pro-apoptotic protein BAX was significantly reduced in DIPG by one-way-ANOVA ($P < 0.05$) (Figure 1a) compared to other pediatric brain tumors. This result was supported by measuring protein levels in our DIPG lines compared to a medulloblastoma line. Baseline levels of BAX were nearly zero in four DIPG cell lines compared to robust baseline expression in the medulloblastoma line (figure 1b). Next, we assessed whether BAX expression levels correlated with patient outcomes. We generated a Kaplan Meier plot for DIPG patients grouped based on BAX expression. (figure 1c). We determined that patients with higher BAX expression have significantly better outcomes compared to patients with lower BAX expression ($P < 0.05$). In order to confirm that the survival

differences were not due to differential expression across subtypes, we measured BAX expression in the molecular subgroups: H3 K27M and H3 WT (figure 1d) and found no significant difference ($p > 0.05$) indicating that this poor survival was not a product of molecular subgroups having different BAX expression. We looked for a survival correlation in other apoptotic proteins including BAK, BCL-2, BCL-xl and MCL-1 but saw no significant correlation between gene expression and clinical outcomes. We measured the levels of BAX as well as its counter pro-survival BCL-2 proteins in response to radiation-induced DNA damage. We irradiated DIPG-13E at 8 Gy and collected lysate at set time points post radiation. 48 h was chosen as the final time point in order to see in changes at the transcriptional level. We confirmed that DNA damage occurred by staining for the DNA damage marker H2AX which was increased 48 h after radiation. BAX expression was barely detectable above background even after radiation (Figure 1e).

**BCL Family Inhibitors Synergize With radiation and Induce Apoptosis in DIPG**

Since BAX expression was reduced in DIPG lines, we hypothesized that we could induce apoptosis by targeting the pro-survival proteins which sequester BAX. BCL-2 family proteins BCL-2, BCL-xl, BCL-W and MCL-1 are responsible for inhibiting BAX and maintaining cell survival. The ratio of these proteins determines cell fate during the DDR. If the pro-apoptotic signal was reduced due to low BAX expression, pharmacologically inhibiting BCL family proteins may help balance the ratio of pro and anti-apoptotic factors. To determine which BCL proteins were involved in survival of DIPG, we screened four BCL inhibitors specific for different targets (Table 1a).

To quantify how synergistic a combination was, we generated a dose response matrix with n =3 for each data point with both radiation and BCL inhibitors (Figure 2a-b). We scored each drug combination

using a zero-interaction potency (ZIP) model (Figure 2c). The ZIP model is based on the assumption that two drugs with zero interaction have no effect on the dose response curve. Using this assumption, the ZIP model calculates a delta score which is the percent deviation from the zero-interaction response. The initial study was done using an autopsy-derived line of DIPG (DIPG-13E). This line was chosen due to its widespread use in other manuscripts are well as its ease of use as a tissue culture model. We quantified the average ZIP score (n =3) and ranked each drug as strongly synergistic (delta ≥ 10), weakly synergistic (delta ≥ 5) or additive (delta < 5). Based on the results (figure 1f) we concluded that navitoclax scored as strongly synergistic, venitoclax scored as weakly synergistic, and both AT101 and S63845 scored as additive. Based on these results we concluded DIPG-13E was sensitive to BCL-2 and BCL-xl inhibition but not inhibition of MCL-1.

These data suggested that navitoclax held the most promise as a radio-sensitizing drug for line DIPG-13E and proceeded to test it in other lines. Further studies included both cell lines derived from treatment-naive patients as well as additional autopsy lines. The treatment-naive lines are more representative of the patient response since these tumors have not accumulated any additional mutations over the course of treatment. The autopsy lines, however, still have some biological relevance and may inform the efficacy of drugs on recurrent tumors that are candidates for re-irradiation. In order to test if this result was representative of DIPG and not line specific, we tested multiple treatment-naive and autopsy lines of DIPG (figure 2d) compared to medulloblastoma lines, which are known to be radiation sensitive, as well as several neural stem cells (NSC). The NSC lines were used to provide insight into the toxicity this combination therapy may have on normal brain tissue. The zip scores were calculated based on three replicates for each point in a dose response matrix for radiation and navitoclax. In addition, the experiment was repeated three times for several lines to confirm reproducibility of the ZIP scores. The combination of navitoclax and radiation in DIPG lines ranged from weakly synergistic (delta > 5) to strongly synergistic (delta > 10). The combination in NSC and medulloblastoma lines ranked as additive (delta < 5).

There was no statistical difference in average ZIP scores between treatment naive DIPG and autopsy DIPG lines by one-way ANOVA ($p > 0.05$). The ZIP scores for both types of DIPG lines were significantly higher compared to medulloblastoma and NSC ($p < 0.05$) (figure 2d).

In order to determine the mechanism by which navitoclax synergizes with radiation, we investigated the cellular response to the combination therapy in lines that exhibited synergy versus lines that did not. We hypothesized that the navitoclax induced apoptosis when combined with radiation in DIPG, while radiation alone was sufficient for apoptosis in the medulloblastoma line that was selected for comparison because it is radiation sensitive. To measure apoptosis, we incubated the target cell lines for both individual treatments and the combination therapy for 48 h then stained using Annexin V FITC and propidium Iodide. The lines used for this experiment represented both the biopsy and autopsy lines, with two lines that had strong synergy in PBT22 and DIPG25F (ZIP > 10) and a weakly synergistic line PBT22 (ZIP > 5). We compared these lines to the medulloblastoma line MED411 which is more sensitize to radiation and did not exhibit synergy (ZIP < 5). The PI stain overlapped entirely with Annexin V stain, so it was not included in this figure. We found the combination of treatments in DIPG lines had significantly higher levels of Annexin V positive cells compared to each treatment individually ($p < 0.01$) while the Med411 showed no significant difference between the combination and radiation alone. Both radiation and the combination in Med411 had close to 100% apoptosis supporting our hypothesis that sensitive lines did not need navitoclax to undergo apoptosis from radiation. Interestingly the line that was weakly synergistic, PBT22, still showed a significant increase in Annexin V positive cells in the combination group. We concluded that lines that showed synergy and a significant increase in apoptosis when exposed to the combination treatment.

**Optimal Dosing Regimen for Combination Therapy**

To inform an *in vivo* study design, we wanted to determine the optimal sequence of radiation and navitoclax, when using these treatments in combination. To test this, we used three different dosing regimens: Navitoclax administered 3 days prior to radiation, radiation administered 3 days prior to navitoclax, and both treatments administered at the same time. We followed the same protocol for calculating ZIP score as used in Figure 1a. Based on the results, we determined that the mean ZIP score was significantly higher when Navitoclax was administered first or the treatment were combined ($p < 0.05$). While pretreatment with Navitoclax had a high ZIP score, the $IC_{50}$ of radiation was reduced compared to the other treatment regimens. We concluded from this experiment that administrating the treatments simultaneously was the optimal regimen.

***In vivo* study to Determine Navitoclax and Radiation Efficacy in a Subcutaneous Model**

We wanted to determine if the synergistic effects of navitoclax and radiation translated to a beneficial therapy *in vivo*. We have previously demonstrated that orthotopic models for DIPG contain an intact Blood Brain Barrier (BBB) which impedes drug delivery. Since Navitoclax is a large hydrophilic molecule, we decided to use a subcutaneous model of DIPG for proof-of-concept experiments to avoid lack of drug delivery as a confounding variable. Subcutaneous models have shown to be representative of orthotopic tumors however it does not complete recapitulate the tumor microenvironment that is seen in the brain. We implanted NSG mice with our *in vivo* model PBT-09 and started treatment enrollment when tumors reached 100 $mm^3$ Based on the results from (figure 3c) we concluded that the most effective dosing regimen was to dose navitoclax concurrently with radiation therapy. Navitoclax was dosed 5 days a week at 100 mg/kg up to 21 doses. Radiation therapy was started after the 3$^{rd}$ dose of navitoclax and

was administered in 2 Gy fractions every other day up to 10 Gy (figure. 4a). To administer the radiation, we used gamma radiation generated from the X-rad in a localized field around the flank tumor. We measured growth a flank tumors 3 times a week until the tumor was removed at 1500 $mm^3$ (figure. 4b). Some of the mice that received radiation however developed mouse leukemia which terminated those samples early. We generated a Kaplan Meier plot that reflects the lifespan until the point of tumor removal. While the study is still ongoing, we found that navitoclax alone has no significant improvement. Radiation and the combo therapy had improvement over the vehicle however it is still unclear if the combo therapy offered a benefit over radiation alone (figure. 4c). In order to account for mice lost to leukemia, we took the recorded the time it took to reach the maximum milestone which flank reached which was 600$mm^3$ (figure. 4d). This study is still ongoing with a second cohort just receiving treatment so the mean difference between the radiation and the combination cohort at the final sample size (n = 10).

**3.4 Discussion:**

In this study, we investigated potential combination therapies that induce apoptosis in DIPG cell lines. A mechanism by which DIPG resists Radiation is the redirection of cell fate from apoptosis to growth arrest. This leaves a large mass of senescent or quiescent cells which drive the tumor recurrence in patients with DIPG. If a therapeutic successfully induced apoptosis in DIPG when combined with radiation, it would increase the efficacy of radiation and potentially prolong survival for DIPG patients. BAX is a frequently reported marker for radiation sensitivity in various tumor lines including adult glioblastomas. BAX is antagonized by pro-survival BCL-2 family protein and the interplay between these two factors is responsible for determining cell fate to DNA damaging events. Based on publicly available data sets of gene expression for BAX in DIPG, we identified that DIPG has reduced levels of BAX expression compared to other common pediatric brain tumors. We also identified that patients whose tumors had low BAX expression have a significantly shorter life expectancy compared to high BAX expression.

DIPG are characterized by epigenetic landscapes that keep the cells in a stem-like state. We speculate that the stem-like characteristic may be responsible for the decreased BAX in DIPG. KO studies of BAX and BCL-xl in mice showed defects in glial development. BAX null mice also showed an abundance of glial and neural stem cells. Researchers concluded that during brain development, the interplay between BAX and BCL-xl control which cells undergo differentiation induced apoptosis. If DIPG maintains the expression profiles of glial stem cells, the low levels of BAX may be a relic of a differentiation program used in brain development.

In order to compensate for the reduced BAX expression in DIPG, we investigated whether drugs that specifically target the BAX BCL-2 interaction were capable of inducing apoptosis in DIPG when given in combination with radiation. We identified navitoclax, a BCL-2, BCL-w and BCL-xl inhibitor, as a drug that synergized with radiation in DIPG. We did not see this synergy in a medulloblastoma model, which is likely due to the fact that this model has sufficient BAX to be radiation responsive. It reasonable that a pan BCL inhibitor was most effective since BCL-2 and BCL-xl are both responsible for inhibiting BAX. Our data suggests that this synergy is the result of navitoclax inducing apoptosis in DIPG when combined with radiation while in medulloblastoma, radiation was sufficient to induce apoptosis. When optimizing the dosing regimen, we determined that administering both radiation and Navitoclax at the same time was more effective than staggering the treatments.

We predict that the window for effective combination therapy is during the DNA damage response when the BAX BCL-2 interplay determines the cell fate. The addition of navitoclax treatment following radiation had a diminished response because it missed this key window. For our *in vivo* study we chose to go with flank tumors since it was unlikely that navitoclax dosed orally would cross the BBB. We have determined from previous studies that growing DIPG in flank is still biologically relevant compared to growing orthotopically. Flanks lack the microenvironmental of an orthotopic model, which could affect our results. When considering this treatment for clinical applications, it is important to determine if the patient has

an intact BBB. A challenge for treatment of DIPG by chemotherapeutics is that DIPG patients frequently have intact BBB. For combination of BCL inhibitors and radiation to be effective in DIPG, a BBB penetrating BCL inhibitor will need to be developed. The BBB penetration limits the immediate therapeutic application of this study, the combination of navitoclax and radiation provides key insights into therapeutic targets for DIPG.

### 3.5 Methods

#### Human specimen and patient-derived cell cultures

Human cell cultures were generated with informed consent in compliance with Institutional Review Board (IRB) approval at Seattle Children's Hospital (#14449), Children's National Medical Center (#1339), and University Children's Hospital Zurich (#2019-00615). PBT-09FH, PBT-22FH, PBT-24FH, PBT-27FH, and DRIz-D105 were biopsy-derived at diagnosis. For PBT-09FH, PBT-22FH, PBT-24FH, PBT-27FH, and MED-114, MED-2112, MED-411 tumor tissue was obtained at Seattle Children's Hospital and cell cultures were created at Fred Hutchinson Cancer Research Center (FHCRC). SU-DIPG4, SU-DIPG13, SU-DIPG25, SU-DIPG33, SU_DIPG36 obtained from Dr. Michelle Monje (Stanford University, Stanford, CA, USA). Cells were maintained in NeuroCult NS-A Basal Medium with NS-A Proliferation Supplement (STEMCELL Technologies; Vancouver, CAN), 1X Antibiotic/Antimycotic (ThermoFisher Scientific; MA, USA), 40 ng/mL epidermal growth factor (PeproTech; NJ, USA), and 40 ng/mL fibroblast growth factor (PeproTech; NJ, USA). All cell culture models were validated by DNA fingerprinting.

#### Antibodies and Western blotting

Cells were lysed in M-PER lysis buffer (ThermoFisher; MA, USA), supplemented with PhosSTOP and cOmplete inhibitors (Sigma-Aldrich; MO, USA) and the protein concentration was measured utilizing QuickStart Bradford 1X Dye Reagent (Bio-Rad; CA, USA). Samples were resolved on Bolt 4-12% Bis-Tris gels (ThermoFisher; MA, USA), transferred to 0.2 µm nitrocellulose. Antibodies

used were β-Tubulin (ab189511) Mouse mAb at 1:5000 (abcam), γ-H2A.X (phosphor S139) Rabbit mAb (EP8542Y) at 1:1000 (abcam), Bcl-xl (54H6) Rabbit mAb at 1:1000 (Cell Signalling), Bcl-2 (ab196495) Rabbit polyclonal at 1:1000 (abcam), BAX (2772) Rabbit mAb at 1:1000 (Cell Signaling). Secondary antibodies from Li-Cor Biosciences (NE, USA) were used at 1:10,000 to detect primaries (IRDye 800CW Donkey anti-Mouse IgG and IRDye 680RD Goat anti-Rabbit IgG).

**Cell viability and apoptosis assays for drug and radiation treatment**

Navitoclax (ABT-263), Venetoclax (ABT-199), AT101 (Gossypol Acetate) and S63845, purchased from Selleckchem (TX, USA). For in vitro drug studies, cells were plated in 96-well plates at 5,000 cells per well and cultured 72 hours in the presence of drug in at least triplicate. Experiments were repeated for validation. Radiation studies were performed using an X-rad 320 Precision X-ray (Precision X-Ray, Inc.; CT, USA) using stage position 4, 320 KV, and 12.50 mA on filter 1. For cell viability studies following radiation, 96-well plates were coated in 10 μg/mL of laminin (Sigma-Aldrich; MO, USA) in DPBS and incubated for > 4 hours, after which 5,000 cells per well of a single-cell suspension were plated, 24 hours later irradiated, then viability was measured 96 hours later. Cell viability was measured using CellTiter-Glo® Luminescent Cell Viability Assay (Promega; WI, USA), and data was collected on a Synergy 2 plate reader (Bio-Tek; VT, USA). Flow cytometry was performed on a NovoCyte Flow Cytometer (ACEA Biosciences; CA, USA) using Annexin V-FITC (Biolegend; CA, USA) and data was analyzed using FlowJo software (Becton-Dickinson; NJ, USA).

**Surgical procedure and in vivo treatment of tumor bearing mice**

Mouse studies were conducted in accordance with FHCRC Institutional Animal Care and Use Committee (IACUC) approved protocol #1457. 8-week-old NOD.Cg-Prkdcscid Il2rgtm1Wjl/SzJ (NSG) mice were provided by internal breeding. Athymic nude (Hsd:Athymic Nude-Foxn1$^{nu}$) mice were obtained from

Envigo (IN, USA). SFlank xenografts were established by injection ~$2x10^6$ dissociated PBT-09 cells into soft tissue flank of athymic nude mice. Navitoclax was dissolved in 2% Tween80, 30% DMSO, 30% Peg300 in water. Mice were dosed 5 days a week up to 21 doses. Radiation studies were performed using an X-rad 320 Precision X-ray (Precision X-Ray, Inc.; CT, USA) using stage position 4, 320 KV, and 12.50 mA on filter 2. Mice received 2 Gy every other day up ato 10 Gy total.

**Statistical Analysis**

IC50 were calculated using a non-linear fit with three variables on PRISM GraphPad. To evaluate differences across groups we used a one-way ANOVA with multiple comparisons test to find significance between groups. ZIP scores were calculated using a 90% confidence index across three technical replicates using synergyfinder.fi generated by Ianevski et al. Kaplan Meier plots were generated in PRISM Graphpard and significance was calculated.

### 3.6 Figures

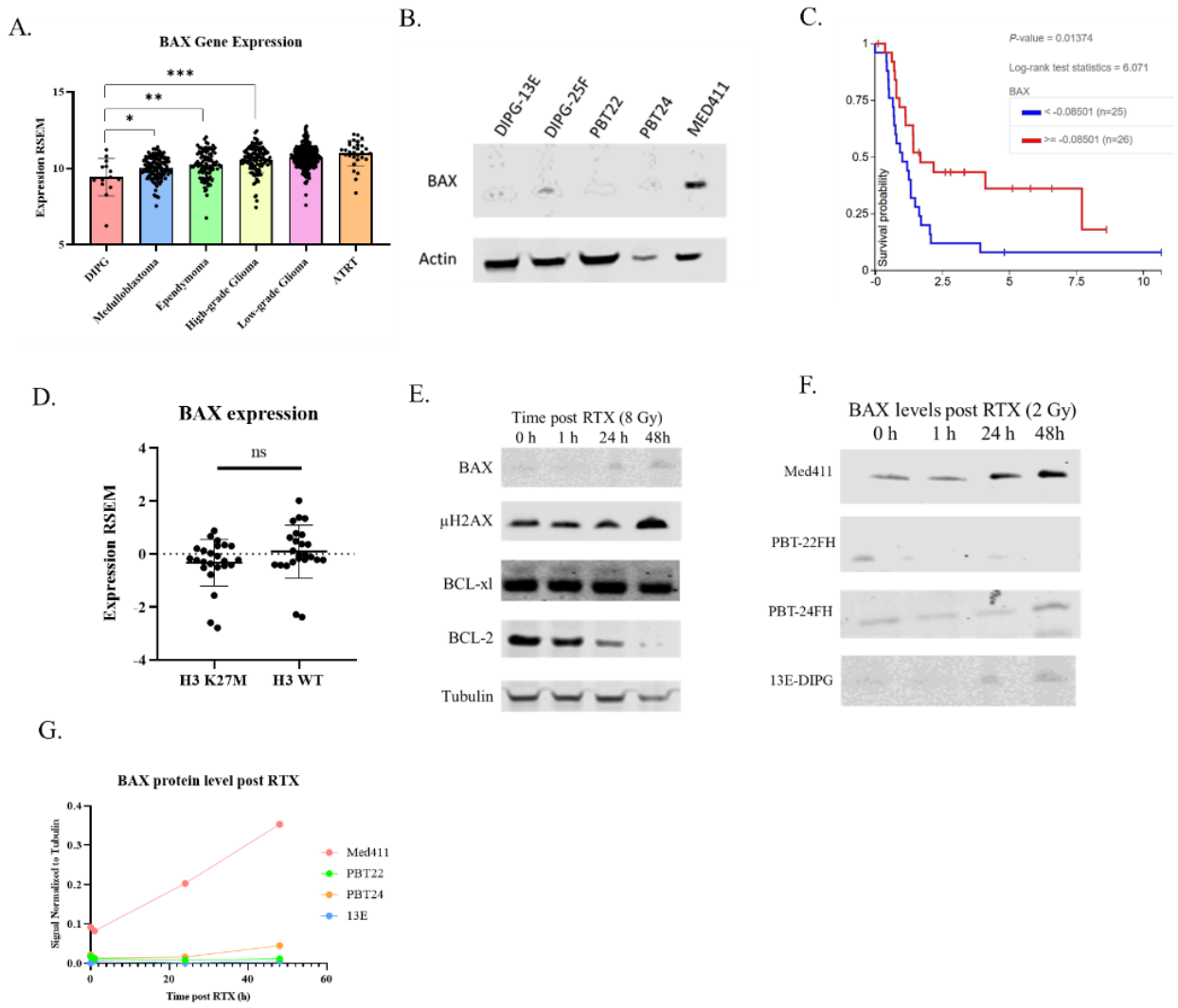


**Figure 1 Legend: BAX protein levels between DIPG and other pediatric brain tumors. (A)** Gene exression levels of BAX measured across most frequent pediatric brain tumors. **(B)** Western blot of DIPG and Medulloblastoma for BAX. **(C)** Survival data of DIPG pateitns with high and low levels of BAX expression. State what the colors indicate. The legend in the figure isn't helpful. **(D)** BAX expression between H3 K27M and H3 WT tumor subtypes. **(E)** Westernblot of key DNA damge repsonse proteins in DIPG-13E at set time points post radiaiotn at 8 Gy. **(F)** Western blot of BAX protein levels across

| | BCL Family Inhibitor $K_i$ | | | |
|---|---|---|---|---|
| Drug: | BCL-2 | BCL-xL | BCL-W | MCL-1 |
| Navitoclax (ABT263) | ++++ | ++++ | ++++ | |
| Venetoclax (ABT199) | ++++ | | | |
| AT101 | ++ | ++ | ++ | +++ |
| S63845 | | | | ++++ |

**Table 1 Legend: BCL inhibitor $K_i$ Values.** $K_i$ values for corresponding BCL proteins (++++ > 1 nM), +++ > 100 nM, ++ > 1μM)

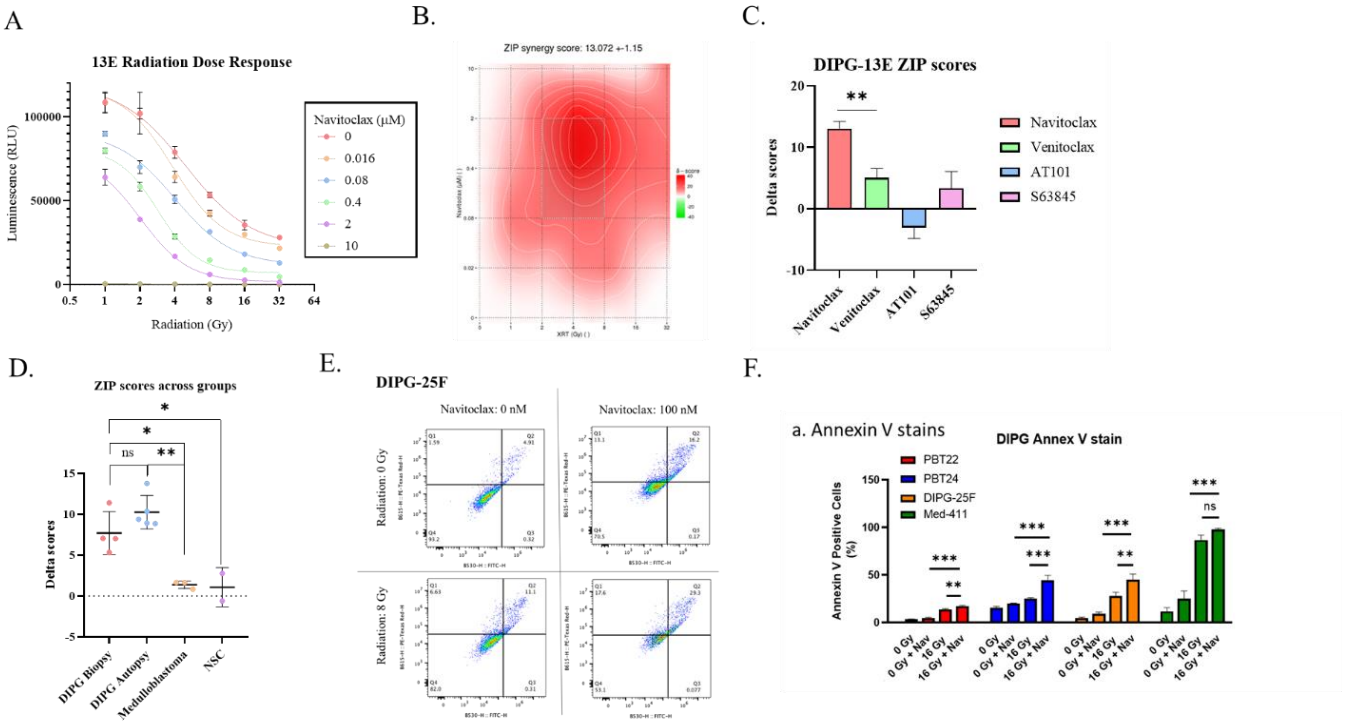


**Figure 2 Legend: Synergy Quantification Between Radiation and BCL2 Family Inhibitors. (A)** Radiation dose response at different constant navitoclax doses. **(B)** Topographic plot of Delta scores generated for each dose combination of Navitoclax and Radiation. **(C)** Average ZIP scores calculated for each BCL inhibitor. **(D)** Average ZIP score across all DIPG biopsy, DIPG autopsy lines, Medulloblastoma and NSC lines. **(E)** Example of annexin V-FTIC vs propidium iodide staining in DIPG 25F at set doses of radiation and navitoclax. **(F)** Average number of Annexin V positive cells across four lines.

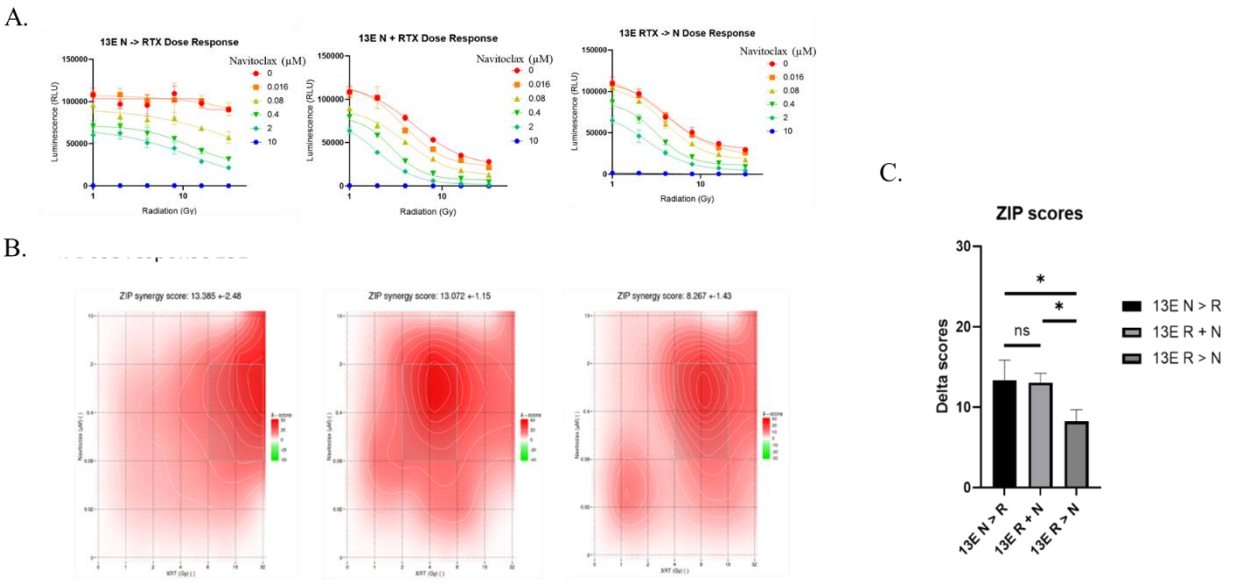


**Figure 3 Legend**: **Radiation Navitoclax Synergy at Different Dosing Regimens.** (**A)** Radiation dose response with Navitoclax administered at different time points. **(B)** Topographical plots of delta scores for different dosing regimens. **(C)** Average Delta scores for each dosing regimen.

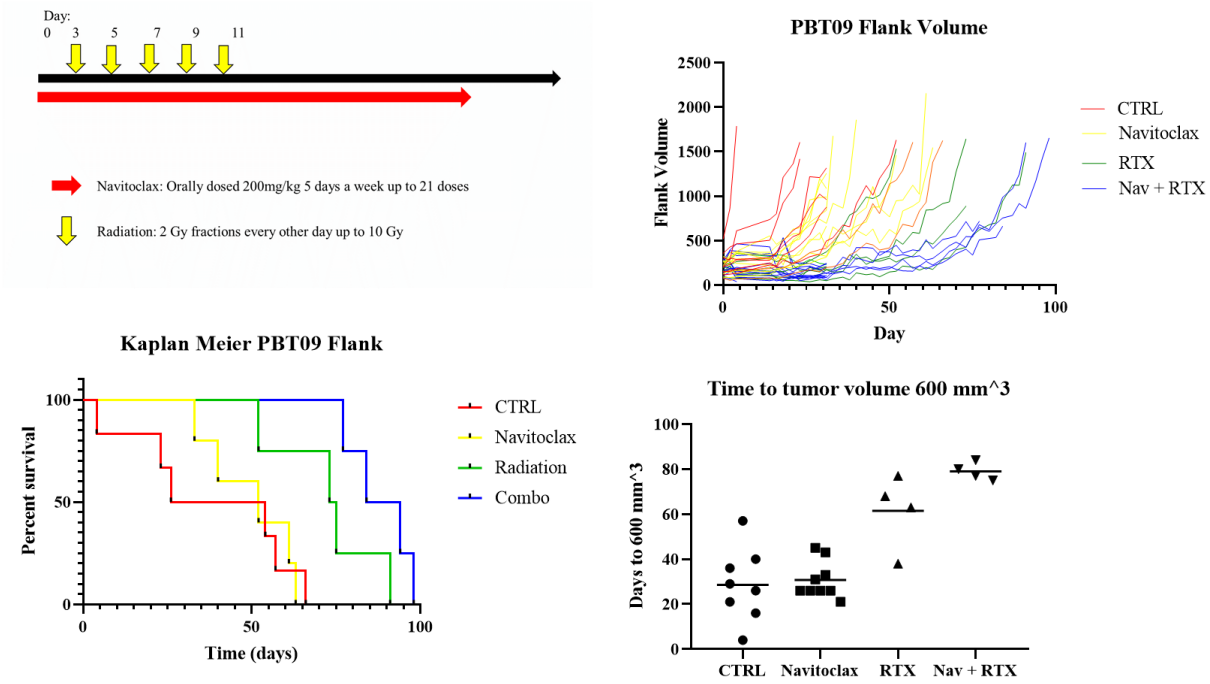


**Figure 4 Legend: In-vivo Dosing of Navitoclax and Radiation Therapy. (A)** Dosing schedule for NSG flank tumors following enrollment. **(B)** Tracking tumor volume in each individual mouse. Color corresponds to treatment group. **(C)** Kaplan Meier plot for tumor removal at 1500 $mm^3$. **(D)** Time in days for tumors to reach the size of 600 $mm^3$.

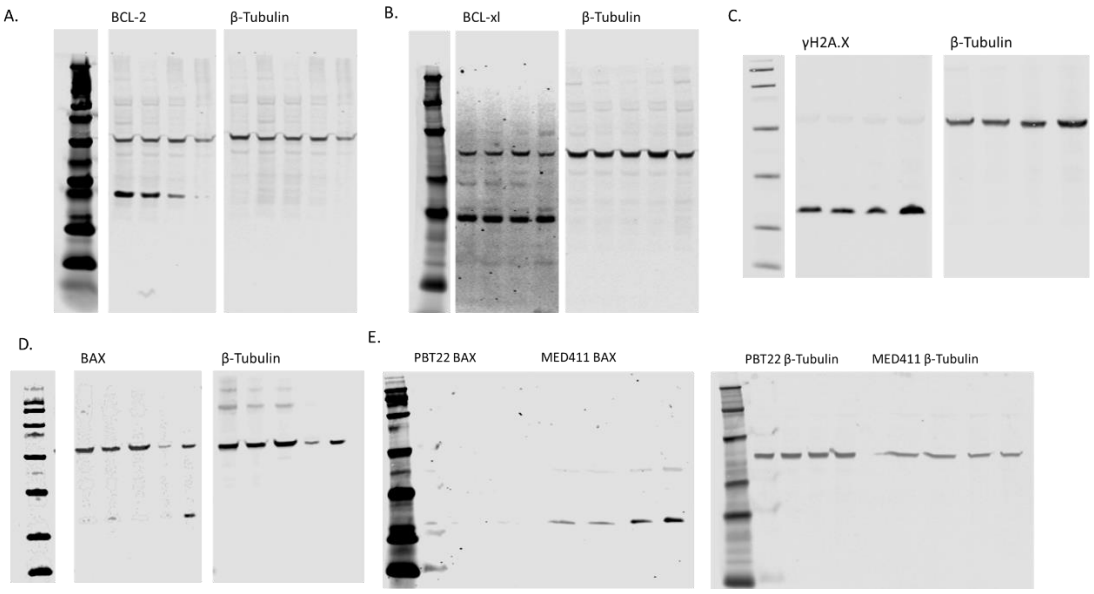


**Supplementary Figure 1 Legend: Raw Western Blot for Figure 3. (A)** 13E with anti BCL-2 post radiation **(B)** 13E with anti BCL-xl post radiation. **(C)** 13E with anti BAX post radiation. **(D)** All DIPG lines with anti BAX **(D)** Med411 and PBT22 with anti BAX post radiation.

## Chapter 4: Conclusion and Future Direction

### 4.1 Abstract:

We have previously shown that radiation dose not induce the expression of the key apoptotic protein BAX in DIPG cells. DIPG differs from other pediatric brain tumors in that it has a unique epigenetic profile stemming from mutations to histone H3. Since the reduced levels of BAX and subsequent resistance to radiation is more pronounced in DIPG compared to other pediatric brain tumors, we predict that the unique epigenetic profile is driving this response. For future direction we will look at several key transcription factors which regulation BAX and how they are impacted by the epigenetics of DIPG cells.

### 4.2 Conclusion

Our research has focused on understanding how DIPG resist conventional therapies such as radiation and chemotherapy. In order to get a better understand of these tumors, we developed a protocol by which to culture treatment naive biopsies. Using these models, we determined that one mechanism by which DIPG resists radiation is by avoiding apoptosis following a DNA damaging event. This work has also been validated by Werbrouck et al who also developed treatment naive biopsy models [50]. They used a different method for assessing radiation dose response, however the range of the IC50 to radiation overlapped with our finding. They saw a similar link between radiation resistance and patient response in clinic. Their conclusion was that p53 mutation status was a key predictor in DIPG response to radiation. While p53 likely contributes to radiation resistance it does not account for several observations including H3.1 K27M DIPG which almost never have p53 mutations but have similar overall survival to H3.3. It also does not account for the discrepancy between DIPG and or pediatric brain tumors which also frequently have mutations to p53.

We concluded that a key mechanism by which DIPG are resistant is the inability to undergo apoptosis. Clinical evaluation of DIPG patients post radiation shows only modest reduction in tumor size suggesting that radiation is not sufficient to kill DIPG cells. While senescence and quiescence has been

previously seen as a positive outcome, recent studies have suggested that large populations of senescent cells and drive tumor recurrence through the secretion of senescent associated secretory phenotype (SASP) [87]. This would help explain why DIPG that reoccur are often more aggressive than the treatment naive tumor. In order to identify mechanisms behind the resistance to apoptosis, we looked at a number of pro-survival and pro-apoptotic proteins using differential expression in DIPG as well survival correlations as a criterion. BAX stood out since it was a key pro-apoptotic regulator that was reduced in DIPG and negatively correlated with poor survival. We compared these tumors to radiation sensitive brain tumors in medulloblastoma and found that BAX was reduced in DIPG and did not accumulate following radiation. The exact mechanism by which BAX expression is suppressed in DIPG is still unclear however specific transcription factors for BAX are reduced in DIPG compared to other pediatric brain tumors. DIPG have unique transcription profiles since the H3 K27M mutation locks in the epigenetic state of the glial stem progenitor cell. Interestingly, studies have suggested that during brain development, the interaction between BAX and BCL-xl play a key role in regulating which cells undergo developmental apoptosis [88]. Mice that were double negative for either BAX or BCL-xl showed significant aberrations to brain development and neuron growth. Since we have observed that DIPG have low levels of BAX and high levels of BCL-xl, it is not unreasonable hat DIPG may have locked in some embryonic program that prevents BAX expression for proper tissue development. Future studies will focus on identifying key transcription factor and epigenetic modifiers to determine if these proteins are driving BAX suppression in DIPG.

### 4.2 Future plans

#### Confirming BAX Role in Treatment Resistance

While we have shown the BAX expression correlates with radiation resistance the next step is to establish causation. In order to demonstrate this causation, we plan to develop a system that we can

artificially induce either BAX or a GFP control in DIPG. We plan to use a Tet on promoter that induces expression depending on the concentration of doxycycline. This will allow us to control BAX expression to avoid any toxicity from over expressing BAX. Once we have a set dose of doxycycline, we will induce either BAX or GFP in radio resistant DIPG lines and measure the percent of cells that undergo apoptosis. We will use an unpaired two tailed Students T-test to assess significance between these groups. We also want to confirm if the resistance to apoptosis in DIPG is specific to radiation or any DNA damaging events. We will repeat this experiment with frequently used chemotherapy agents such as temozolomide and doxorubicin to determine if BAX protein levels drive resistance to other therapies as well. These experiments with confirm if BAX is directly linked to radiation resistance. Follow experiments will focus on why BAX is dysregulated in DIPG compared to other pediatric brain tumors. We will also screen for additional drug libraries using BAX expression as a reporter for drugs which will improve radiation efficacy.

**Mechanism Behind BAX Regulation**

Since we observed BAX mRNA differences between DIPG and other pediatric brain tumors we concluded that regulation was occurring at the transcriptional level. Regulation of BAX levels is used to control cell fate following a DNA damage response. When BAX dimerizes with BID at the mitochondrial membrane, it forms a pore that releases cytochrome c. At this stage, the apoptotic pathway is irreversible, making the BAX-BAK dimerization the final regulatory step for determining cell fate. Pro-survival BCL2 proteins including BCL-2, BCL-xl and MCL-1 sequester BAX and prevent dimerization with BID [89]. Additional pro-apoptotic proteins like NOXA and PUMA act as competitive inhibitors by binding to BCL-2 family proteins, preventing the sequestration of BAX [90]. This process is extremely dynamic and relies on very precise levels of protein to determine the appropriate cell fate.

When treating tumors, apoptosis is the optimal end goal because quiescent and senescent cells have been shown to drive tumor recurrence[87]. Tumors that can avoid apoptosis by down regulating

pro-apoptosis proteins such as BAX, are more resistant to conventional therapies such as radiation and chemo. Previous studies in adult GBM have found that histological levels of BAX were predictive of worse patient outcomes. Evaluation of other tumors such as esophageal carcinoma and prostate cancer use BAX and BCL-2 as a biomarker to determine is radiation will be effective [91-93]. Understanding how tumors suppress BAX may lead to therapies which upregulate BAX and sensitize tumors to radiation. DIPG follows this trend of low BAX expression driving resistance to radiation. A unique feature of DIPG is the altered expression profiles due to the changes in epigenetics from the H3 K27M mutation [20]. This mutation prevents the silencing of specific genes by the PRC 2, but also leave chromatin which already contained the repressive marks H3 K27me3 remain repressed. Studies have shown that genes which are repressed by H3 K27me3 like CDKN2A are unable to become derepressed unless treated with the demethylase EZH2 inhibitor [24]. Since BAX mRNA levels were reduced in DIPG compared to other brain tumors, we hypothesized that the regulation was at the transcriptional level and driven by the unique epigenetics of DIPG.

**Epigenetic Regulation of BAX**

The epigenetic state of BAX is unknown in H3 K27M tumors, so we wanted to identify the epigenetic state of the BAX gene loci. Using a technique known as Cut n Run, we mapped the location of specific epigenetic markers in the genome of DIPG cells. Cut and Run is similar to Chip-seq however rather than fracturing DNA for immunoprecipitation, Cut n Run uses a secondary antibody fused to the DNase: MNase [94]. When calcium is added, the MNase cleaves the DNA strand around the antibody protein complex allowing for passive excision of that DNA segment (Figure 4.1a). Cut n Run is higher throughput compared to ChIP-Seq and does not have as high of background noise which occurs when DNA is manually fractured during ChIP-Seq. Analysis of the BAX loci in the H3.3 K27M mutated DIPG lines PBT22 showed relatively low modifications on the histones surrounding BAX (Figure 4.2). BAX gene loci did not contain the repressive marker H3 K27me3, but it also lacked markers of active transcription such as H3 K4me3,

H3 K27ac, and H3.3 K27M mutant which accumulates at sites of active transcription. The only mark present above background was H3 K4me1 which typically indicates active enhancer sites. The BAX gene is known to be regulated by GFI1 or GFI1b which is a scaffold for HDAC and Demethylases such as LSD1 which blocks H3 K4me3 and H3 K27ac [95, 96]. TP53 inhibits expression of GFI1 allowing for the accumulation of active marks [97]. Interestingly knockdown of LSD1 has been shown to synergize with other treatments such as HDACi and corrin in DIPG-13E which we previously shown to have reduce BAX [98]. While this study did not look at LSD1 inhibitors in combination with radiation it is a potential future target for upregulating BAX in DIPG. GFI1 and GFIb which coordinate LSD1 are also regulated by the PRC2 which is inhibited by H3 K27M. Interestingly GFI1 contains the repressive marker H3 K27me3 in both DIPG and Medulloblastoma but GFI1b has significantly reduced K27me3 reads in DIPG (Figure 4.1b). Future studies will look at GFIb protein levels across DIPG and Medulloblastoma. If there is a significant difference, we will determine if knocking out GFIb increases BAX expression and sensitizes DIPG to radiation. Additional drug candidates such as LSD1 and HDAC inhibitors will also be explored as potential radio-sensitizing agents.

**Transcription Factors Which Regulate BAX**

Another mechanism by which BAX is regulated is through its transcription factors. We speculated that BAX expression may be controlled by an embryonic program used to control which cells undergo apoptosis during development. These programs are usually carried out by multiple transcription factors which drive the observed phenotypes. In order to identify regulator elements, we used the PROMO algorithm developed by ALGGEN research group which predicts transcription factors (TF) that bind to a given segment of DNA. We used the promoter region of BAX from +100 to -1000 from the TATA box. We identified 45 TF that were predicted to bind to the BAX promoter. This included both transcriptional activators such as TP53 and suppressors such as ETS1. We used the JASPAR Core Promoter library to validate that these binding motifs existed in the BAX promoter. Next, we wanted to determine if these TF

were dysregulated in DIPG. Using the database for pediatric brain tumors CBTTC, we obtained data for gene expression levels of these transcription factors across all pediatric brain tumors. We compared the fold change between DIPG to radiosensitive tumors in Medulloblastoma as well as the average among all pediatric brain tumors (Figure 4.2B). To assess the validity of the fold changes we conducted a two tailed t-test between the mean expression levels of DIPG and Medulloblastoma. We identified several TF that were significantly higher in Medulloblastoma including the transcriptional activators HNF1B and PAX5, which have been demonstrated to induce apoptosis when overexpressed. The Cut n Run assays showed presence of the repressive marker H3 K27me3 at the promoter of both HNF1B and PAX5 in DIPG (Figure 4.2 B,C). Although DIPG is characterized by markedly reduced H3 K27me3, research has shown some regions remain repressed such as the tumor suppressor CDKN2A. We also found the repressor ETS1 to be upregulated in DIPG. ETS1 had an active chromatin landscape with high levels of H3 K4me1 and H3 K27M.

Regardless of the mechanism by which DIPG resist apoptosis, this phenomenon makes treating DIPG a difficult proposition. While BCL inhibitors have been shown to improve the efficacy of radiation in laboratory conditions, it is unclear if this will translate to a clinical setting. This is compounded by that fact that many DIPG patients have an intact blood brain barrier so few treatments would be BBB penetrant. While navitoclax increases the strength of the pro-apoptotic signal by inhibiting BCL-2 proteins, it does not target the problem of de-repressing BAX in DIPG. Going forward there may be epigenetic drugs which are capable of restoring BAX gene expression. Future drug screens should use BAX expression of a biomarker for a successful combination therapy. Hopefully, the more we understand about why DIPG is so resistant to therapy, the better we will be able to target this and improve clinical outcomes.

### 4.3 Material and Methods

**Cell Culture:**

Human cell cultures were generated with informed consent in compliance with Institutional Review Board (IRB) approval at Seattle Children's Hospital (#14449). PBT-22FH was biopsy-derived at diagnosis, MED-411 tumor tissue was obtained at Seattle Children's Hospital and cell cultures were created at Fred Hutchinson Cancer Research Center (FHCRC). SU-DIPG4 and SU-DIPG13, from Dr. Michelle Monje (Stanford University, Stanford, CA, USA). Cells were maintained in NeuroCult NS-A Basal Medium with NS-A Proliferation Supplement (STEMCELL Technologies; Vancouver, CAN), 1X Antibiotic/Antimycotic (ThermoFisher Scientific; MA, USA), 40 ng/mL epidermal growth factor (PeproTech; NJ, USA), and 40 ng/mL fibroblast growth factor (PeproTech; NJ, USA). All cell culture models were validated by DNA fingerprinting. Drosophila S2 cells obtained were grown in HYQ-SFX insect medium (ThermoFisher). Cells grown two days before use as internal control for Cut & Run.

**Cut&Run**

CUT&RUN was performed as described Skene et al., 2018. Antiboies were diluted at 1:100. All cells were counted on the ViCell (ThermoFisher). Droisphila S2 cells were used as a spike at a ration of 1:20. DNA was prepped by the method used in Skene and Henikoff 2017. Sequencing reads were mapped to the human hg19 genome build. The bedgraph file of human reads were normalized to spike reads based on initial input ratio.

## 4.3 Figures

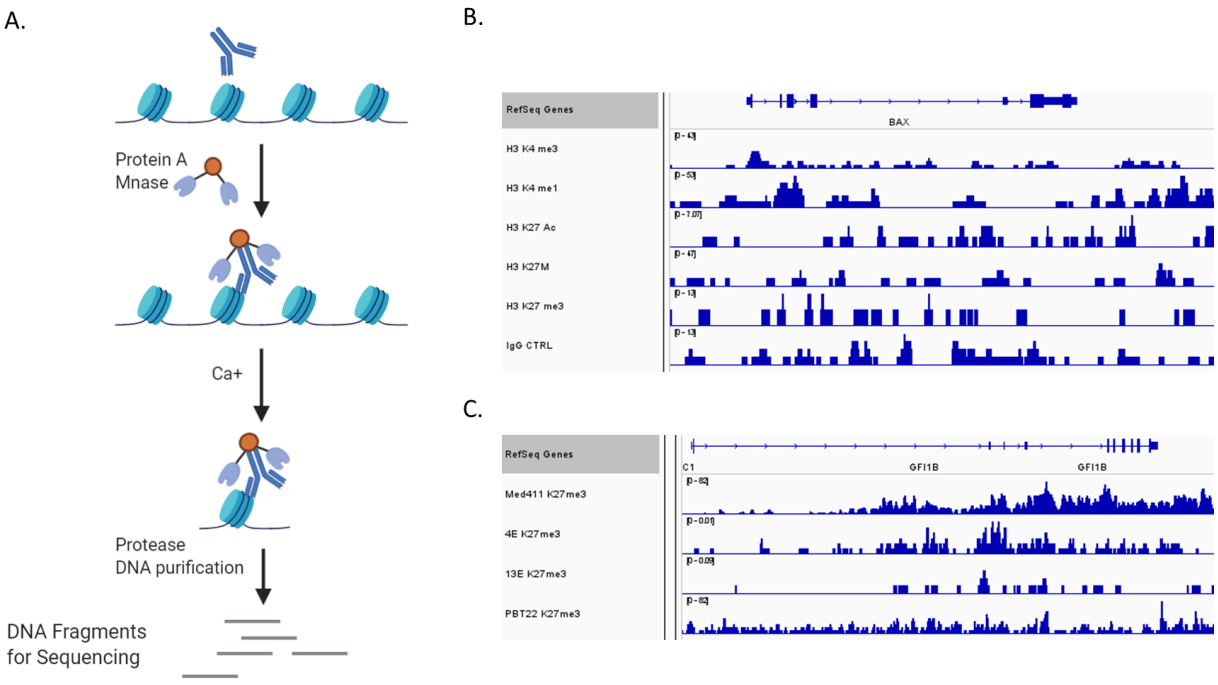


**Figure 1 Legend: CUN and RUN Reveals Epigenetic Regulation of Genes in DIPG: (A)** Schematic of Cut and Run protocol for purification of DNA fragments corresponding to specific DNA binding targets. **(B)** IGV track for read counts corresponding to specific histone modifications in PBT22 at the BAX loci. IgG serves as control for background noise. All counts normalized to spike DNA to control for cell numbers. **(C)** Read counts corresponding to H3 K27 me3 sites at the GFI1b loci. Corresponding cells included are Med411, DIPG-4E. DIPG-13E and PBT22.

| TF Predicted for BAX Promoter | Fold Change vs. Medulloblastoma | Mean Difference (P Value) | Fold change vs. all pediatric brain tumors | Mean Difference (P Value) |
|---|---|---|---|---|
| HNF1B | 0.164 | 0.002 | 0.254 | 0.057 |
| CRX | 0.263 | 0.000 | 0.886 | 0.772 |
| PAX5 | 0.269 | 0.000 | 0.567 | 0.018 |
| HNF4A | 0.322 | 0.030 | 0.390 | 0.100 |
| POU1F1 | 0.535 | 0.614 | 0.564 | 0.646 |
| GATA1 | 0.581 | 0.269 | 0.400 | 0.043 |
| MYB | 0.634 | 0.000 | 1.014 | 0.916 |
| FOXP3 | 0.775 | 0.001 | 0.757 | 0.000 |
| E2F1 | 0.783 | 0.000 | 0.976 | 0.648 |
| STAT4 | 0.813 | 0.038 | 0.853 | 0.054 |
| HOXD8 | 0.876 | 0.582 | 0.835 | 0.429 |
| GTF2I | 0.911 | 0.000 | 0.958 | 0.005 |
| GCFC2 | 0.918 | 0.000 | 0.951 | 0.019 |
| ESR1 | 0.918 | 0.272 | 0.732 | 0.000 |
| ELK1 | 0.922 | 0.000 | 0.942 | 0.005 |
| MAZ | 0.925 | 0.000 | 0.990 | 0.581 |
| YY1 | 0.947 | 0.000 | 0.960 | 0.004 |
| ARNT | 0.952 | 0.001 | 0.967 | 0.049 |
| AP2A1 | 0.956 | 0.011 | 0.939 | 0.000 |
| TP53 | 0.961 | 0.176 | 0.961 | 0.139 |
| NFYA | 0.962 | 0.054 | 1.011 | 0.554 |
| SP1 | 0.972 | 0.071 | 0.967 | 0.042 |
| USF2 | 0.979 | 0.184 | 0.967 | 0.046 |
| RARB | 0.981 | 0.777 | 0.874 | 0.011 |
| TCF4 | 0.991 | 0.700 | 0.996 | 0.841 |
| LEF1 | 0.997 | 0.963 | 0.932 | 0.134 |
| NFKB1 | 0.997 | 0.909 | 0.950 | 0.021 |
| STAT1 | 0.999 | 0.956 | 0.932 | 0.004 |
| MYOD1 | 1.028 | 0.895 | 2.070 | 0.002 |
| IRF2 | 1.033 | 0.087 | 0.964 | 0.109 |
| SREBF1 | 1.038 | 0.195 | 0.916 | 0.004 |
| CACYBP | 1.072 | 0.000 | 1.093 | 0.000 |
| ETS2 | 1.092 | 0.000 | 0.991 | 0.745 |
| JUN | 1.100 | 0.000 | 1.025 | 0.324 |
| NR3C1 | 1.102 | 0.002 | 0.984 | 0.522 |
| IKZF1 | 1.116 | 0.008 | 0.885 | 0.016 |
| RXRA | 1.161 | 0.000 | 1.011 | 0.667 |
| IRF1 | 1.167 | 0.000 | 0.989 | 0.761 |
| ETS1 | 1.175 | 0.000 | 1.027 | 0.393 |
| CEBPA | 1.204 | 0.000 | 0.963 | 0.419 |
| AHR | 1.235 | 0.000 | 1.011 | 0.810 |
| NR1I2 | 1.339 | 0.012 | 0.996 | 0.968 |
| VDR | 1.378 | 0.000 | 1.074 | 0.396 |
| HNF1A | 2.414 | 0.000 | 2.187 | 0.000 |

**Table 1 Legend: Transcription Factors Predicted to Bind to BAX Promoter:** Transcription Factors predicted within a dissimilarity of 8 to bind to the BAX promoter from +100 to -1000 from the TATA box. Ranking is based on differential gene expression between DIPG and Medulloblastoma. Statistics of differential expression based on unpaired two tailed Student's T-test. Expression also compared to all pediatric brain tumors in CBTTC cohort using same statistics and previously mentioned.

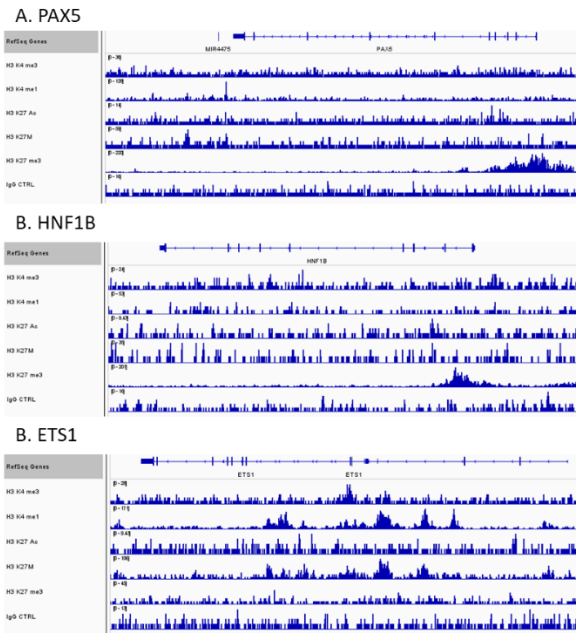


**Figure 2 Legend: IGV Tracks of Gene Loci for Transcription Factors Predicted to Regulate BAX: (A)** IGV track for PAX5 gene loci in PBT22. Auto scaled based on read counts with IgG CTRL. **(B)** IGV track for HNF1B gene loci in PBT22. **(C)** IGV track for ETS1 gene loci in PBT22.

1. Johnson, K.J., et al., *Childhood brain tumor epidemiology: a brain tumor epidemiology consortium review.* Cancer Epidemiol Biomarkers Prev, 2014. **23**(12): p. 2716-36.
2. Mackay, A., et al., *Integrated Molecular Meta-Analysis of 1,000 Pediatric High-Grade and Diffuse Intrinsic Pontine Glioma.* Cancer Cell, 2017. **32**(4): p. 520-537 e5.
3. Ostrom, Q.T., et al., *CBTRUS Statistical Report: Primary Brain and Other Central Nervous System Tumors Diagnosed in the United States in 2009-2013.* Neuro Oncol, 2016. **18**(suppl_5): p. v1-v75.
4. Nishikawa, R., *Pediatric and adult gliomas: how different are they?* Neuro Oncol, 2010. **12**(12): p. 1203-4.
5. Danielsson, A., et al., *MethPed: a DNA methylation classifier tool for the identification of pediatric brain tumor subtypes.* Clin Epigenetics, 2015. **7**: p. 62.
6. Holland, E.C., *Progenitor cells and glioma formation.* Curr Opin Neurol, 2001. **14**(6): p. 683-8.
7. Lindberg, N., et al., *Oligodendrocyte progenitor cells can act as cell of origin for experimental glioma.* Oncogene, 2009. **28**(23): p. 2266-75.
8. Jansen, M.H., et al., *Diffuse intrinsic pontine gliomas: a systematic update on clinical trials and biology.* Cancer Treat Rev, 2012. **38**(1): p. 27-35.
9. Jansen, M.H., et al., *Survival prediction model of children with diffuse intrinsic pontine glioma based on clinical and radiological criteria.* Neuro Oncol, 2015. **17**(1): p. 160-6.
10. Fangusaro, J., *Pediatric high grade glioma: a review and update on tumor clinical characteristics and biology.* Front Oncol, 2012. **2**: p. 105.
11. Schwartzentruber, J., et al., *Driver mutations in histone H3.3 and chromatin remodelling genes in paediatric glioblastoma.* Nature, 2012. **482**(7384): p. 226-31.
12. Wu, G., et al., *Somatic histone H3 alterations in pediatric diffuse intrinsic pontine gliomas and non-brainstem glioblastomas.* Nat Genet, 2012. **44**(3): p. 251-3.
13. Lu, V.M., et al., *Impact of the H3K27M mutation on survival in pediatric high-grade glioma: a systematic review and meta-analysis.* J Neurosurg Pediatr, 2018. **23**(3): p. 308-316.
14. Louis, D.N., et al., *The 2016 World Health Organization Classification of Tumors of the Central Nervous System: a summary.* Acta Neuropathol, 2016. **131**(6): p. 803-20.
15. Grobner, S.N., et al., *The landscape of genomic alterations across childhood cancers.* Nature, 2018. **555**(7696): p. 321-327.
16. Bogliotti, Y.S. and P.J. Ross, *Mechanisms of histone H3 lysine 27 trimethylation remodeling during early mammalian development.* Epigenetics, 2012. **7**(9): p. 976-81.
17. Laugesen, A., J.W. Hojfeldt, and K. Helin, *Molecular Mechanisms Directing PRC2 Recruitment and H3K27 Methylation.* Mol Cell, 2019. **74**(1): p. 8-18.
18. Lavarone, E., C.M. Barbieri, and D. Pasini, *Dissecting the role of H3K27 acetylation and methylation in PRC2 mediated control of cellular identity.* Nat Commun, 2019. **10**(1): p. 1679.
19. Justin, N., et al., *Structural basis of oncogenic histone H3K27M inhibition of human polycomb repressive complex 2.* Nat Commun, 2016. **7**: p. 11316.
20. Harutyunyan, A.S., et al., *H3K27M induces defective chromatin spread of PRC2-mediated repressive H3K27me2/me3 and is essential for glioma tumorigenesis.* Nat Commun, 2019. **10**(1): p. 1262.
21. Anderson, J.L., et al., *The transcription factor Olig2 is important for the biology of diffuse intrinsic pontine gliomas.* Neuro Oncol, 2017. **19**(8): p. 1068-1078.
22. Nagaraja, S., et al., *Transcriptional Dependencies in Diffuse Intrinsic Pontine Glioma.* Cancer Cell, 2017. **31**(5): p. 635-652 e6.
23. Stafford, J.M., et al., *Multiple modes of PRC2 inhibition elicit global chromatin alterations in H3K27M pediatric glioma.* Sci Adv, 2018. **4**(10): p. eaau5935.
24. Cordero, F.J., et al., *Histone H3.3K27M Represses p16 to Accelerate Gliomagenesis in a Murine Model of DIPG.* Mol Cancer Res, 2017. **15**(9): p. 1243-1254.

25. Pathania, M., et al., *H3.3(K27M) Cooperates with Trp53 Loss and PDGFRA Gain in Mouse Embryonic Neural Progenitor Cells to Induce Invasive High-Grade Gliomas.* Cancer Cell, 2017. **32**(5): p. 684-700 e9.
26. Welby, J.P., et al., *Current Murine Models and New Developments in H3K27M Diffuse Midline Gliomas.* Front Oncol, 2019. **9**: p. 92.
27. Lowe, B.R., et al., *Histone H3 Mutations: An Updated View of Their Role in Chromatin Deregulation and Cancer.* Cancers (Basel), 2019. **11**(5).
28. Martire, S. and L.A. Banaszynski, *The roles of histone variants in fine-tuning chromatin organization and function.* Nat Rev Mol Cell Biol, 2020. **21**(9): p. 522-541.
29. Hoeman, C.M., et al., *ACVR1 R206H cooperates with H3.1K27M in promoting diffuse intrinsic pontine glioma pathogenesis.* Nat Commun, 2019. **10**(1): p. 1023.
30. Castel, D., et al., *Transcriptomic and epigenetic profiling of 'diffuse midline gliomas, H3 K27M-mutant' discriminate two subgroups based on the type of histone H3 mutated and not supratentorial or infratentorial location.* Acta Neuropathol Commun, 2018. **6**(1): p. 117.
31. Yadav, R.K., et al., *Histone H3G34R mutation causes replication stress, homologous recombination defects and genomic instability in S. pombe.* Elife, 2017. **6**.
32. Castel, D., et al., *Histone H3 wild-type DIPG/DMG overexpressing EZHIP extend the spectrum diffuse midline gliomas with PRC2 inhibition beyond H3-K27M mutation.* Acta Neuropathol, 2020. **139**(6): p. 1109-1113.
33. Pratt, D., et al., *Diffuse intrinsic pontine glioma-like tumor with EZHIP expression and molecular features of PFA ependymoma.* Acta Neuropathol Commun, 2020. **8**(1): p. 37.
34. Jain, S.U., et al., *PFA ependymoma-associated protein EZHIP inhibits PRC2 activity through a H3 K27M-like mechanism.* Nat Commun, 2019. **10**(1): p. 2146.
35. Hubner, J.M., et al., *EZHIP/CXorf67 mimics K27M mutated oncohistones and functions as an intrinsic inhibitor of PRC2 function in aggressive posterior fossa ependymoma.* Neuro Oncol, 2019. **21**(7): p. 878-889.
36. Rechberger, J.S., et al., *Clinical trials for diffuse intrinsic pontine glioma: the current state of affairs.* Childs Nerv Syst, 2020. **36**(1): p. 39-46.
37. Kambhampati, M., et al., *A standardized autopsy procurement allows for the comprehensive study of DIPG biology.* Oncotarget, 2015. **6**(14): p. 12740-7.
38. Lin, G.L. and M. Monje, *A Protocol for Rapid Post-mortem Cell Culture of Diffuse Intrinsic Pontine Glioma (DIPG).* J Vis Exp, 2017(121).
39. Caretti, V., et al., *Human pontine glioma cells can induce murine tumors.* Acta Neuropathol, 2014. **127**(6): p. 897-909.
40. Misuraca, K.L., F.J. Cordero, and O.J. Becher, *Pre-Clinical Models of Diffuse Intrinsic Pontine Glioma.* Front Oncol, 2015. **5**: p. 172.
41. Grasso, C.S., et al., *Functionally defined therapeutic targets in diffuse intrinsic pontine glioma.* Nat Med, 2015. **21**(6): p. 555-9.
42. Nikbakht, H., et al., *Spatial and temporal homogeneity of driver mutations in diffuse intrinsic pontine glioma.* Nat Commun, 2016. **7**: p. 11185.
43. Orsulic, S., *An RCAS-TVA-based approach to designer mouse models.* Mamm Genome, 2002. **13**(10): p. 543-7.
44. Misuraca, K.L., et al., *A Novel Mouse Model of Diffuse Intrinsic Pontine Glioma Initiated in Pax3-Expressing Cells.* Neoplasia, 2016. **18**(1): p. 60-70.
45. Halvorson, K.G., et al., *A high-throughput in vitro drug screen in a genetically engineered mouse model of diffuse intrinsic pontine glioma identifies BMS-754807 as a promising therapeutic agent.* PLoS One, 2015. **10**(3): p. e0118926.

46. Katagi, H., et al., *Radiosensitization by Histone H3 Demethylase Inhibition in Diffuse Intrinsic Pontine Glioma.* Clin Cancer Res, 2019. **25**(18): p. 5572-5583.
47. Puget, S., et al., *Biopsy in a series of 130 pediatric diffuse intrinsic Pontine gliomas.* Childs Nerv Syst, 2015. **31**(10): p. 1773-80.
48. Williams, J.R., et al., *Progress in diffuse intrinsic pontine glioma: advocating for stereotactic biopsy in the standard of care.* Neurosurg Focus, 2020. **48**(1): p. E4.
49. Azad, T.D., et al., *Liquid biopsy for pediatric diffuse midline glioma: a review of circulating tumor DNA and cerebrospinal fluid tumor DNA.* Neurosurg Focus, 2020. **48**(1): p. E9.
50. Werbrouck, C., et al., *TP53 Pathway Alterations Drive Radioresistance in Diffuse Intrinsic Pontine Gliomas (DIPG).* Clin Cancer Res, 2019. **25**(22): p. 6788-6800.
51. Baumann, M., et al., *Radiation oncology in the era of precision medicine.* Nat Rev Cancer, 2016. **16**(4): p. 234-49.
52. Morgan, H.E. and D.J. Sher, *Adaptive radiotherapy for head and neck cancer.* Cancers Head Neck, 2020. **5**: p. 1.
53. Gallitto, M., et al., *Role of Radiation Therapy in the Management of Diffuse Intrinsic Pontine Glioma: A Systematic Review.* Adv Radiat Oncol, 2019. **4**(3): p. 520-531.
54. Park, J., J.W. Yea, and J.W. Park, *Hypofractionated radiotherapy versus conventional radiotherapy for diffuse intrinsic pontine glioma: A systematic review and meta-analysis.* Medicine (Baltimore), 2020. **99**(42): p. e22721.
55. Wodarz, D., R. Sorace, and N.L. Komarova, *Dynamics of cellular responses to radiation.* PLoS Comput Biol, 2014. **10**(4): p. e1003513.
56. Jeggo, P.A. and M. Lobrich, *DNA double-strand breaks: their cellular and clinical impact?* Oncogene, 2007. **26**(56): p. 7717-9.
57. Jackson, S.P. and J. Bartek, *The DNA-damage response in human biology and disease.* Nature, 2009. **461**(7267): p. 1071-8.
58. Goldstein, M. and M.B. Kastan, *The DNA damage response: implications for tumor responses to radiation and chemotherapy.* Annu Rev Med, 2015. **66**: p. 129-43.
59. Mao, Z., et al., *Comparison of nonhomologous end joining and homologous recombination in human cells.* DNA Repair (Amst), 2008. **7**(10): p. 1765-71.
60. Patil, M., N. Pabla, and Z. Dong, *Checkpoint kinase 1 in DNA damage response and cell cycle regulation.* Cell Mol Life Sci, 2013. **70**(21): p. 4009-21.
61. Bartek, J. and J. Lukas, *Chk1 and Chk2 kinases in checkpoint control and cancer.* Cancer Cell, 2003. **3**(5): p. 421-9.
62. Smith, H.L., et al., *DNA damage checkpoint kinases in cancer.* Expert Rev Mol Med, 2020. **22**: p. e2.
63. Zhang, X.P., F. Liu, and W. Wang, *Two-phase dynamics of p53 in the DNA damage response.* Proc Natl Acad Sci U S A, 2011. **108**(22): p. 8990-5.
64. Villunger, A., et al., *p53- and drug-induced apoptotic responses mediated by BH3-only proteins puma and noxa.* Science, 2003. **302**(5647): p. 1036-8.
65. Westphal, D., et al., *Molecular biology of Bax and Bak activation and action.* Biochim Biophys Acta, 2011. **1813**(4): p. 521-31.
66. Lord, C.J. and A. Ashworth, *The DNA damage response and cancer therapy.* Nature, 2012. **481**(7381): p. 287-94.
67. Pawlik, T.M. and K. Keyomarsi, *Role of cell cycle in mediating sensitivity to radiotherapy.* Int J Radiat Oncol Biol Phys, 2004. **59**(4): p. 928-42.
68. Mueller, S., et al., *Targeting Wee1 for the treatment of pediatric high-grade gliomas.* Neuro Oncol, 2014. **16**(3): p. 352-60.

69. Caretti, V., et al., *WEE1 kinase inhibition enhances the radiation response of diffuse intrinsic pontine gliomas.* Mol Cancer Ther, 2013. **12**(2): p. 141-50.
70. Montero, J. and A. Letai, *Why do BCL-2 inhibitors work and where should we use them in the clinic?* Cell Death Differ, 2018. **25**(1): p. 56-64.
71. Bailey, S., et al., *Diffuse intrinsic pontine glioma treated with prolonged temozolomide and radiotherapy--results of a United Kingdom phase II trial (CNS 2007 04).* Eur J Cancer, 2013. **49**(18): p. 3856-62.
72. Kossatz, S., et al., *Biomarker-Based PET Imaging of Diffuse Intrinsic Pontine Glioma in Mouse Models.* Cancer Res, 2017. **77**(8): p. 2112-2123.
73. Chornenkyy, Y., et al., *Poly-ADP-Ribose Polymerase as a Therapeutic Target in Pediatric Diffuse Intrinsic Pontine Glioma and Pediatric High-Grade Astrocytoma.* Mol Cancer Ther, 2015. **14**(11): p. 2560-8.
74. Cole, K.A., et al., *Phase I Clinical Trial of the Wee1 Inhibitor Adavosertib (AZD1775) with Irinotecan in Children with Relapsed Solid Tumors: A COG Phase I Consortium Report (ADVL1312).* Clin Cancer Res, 2020. **26**(6): p. 1213-1219.
75. Balakrishnan, I., et al., *Senescence Induced by BMI1 Inhibition Is a Therapeutic Vulnerability in H3K27M-Mutant DIPG.* Cell Rep, 2020. **33**(3): p. 108286.
76. Kumar, S.S., et al., *BMI-1 is a potential therapeutic target in diffuse intrinsic pontine glioma.* Oncotarget, 2017. **8**(38): p. 62962-62975.
77. Panditharatna, E., et al., *Clinicopathology of diffuse intrinsic pontine glioma and its redefined genomic and epigenomic landscape.* Cancer Genet, 2015. **208**(7-8): p. 367-73.
78. Clouaire, T., et al., *Comprehensive Mapping of Histone Modifications at DNA Double-Strand Breaks Deciphers Repair Pathway Chromatin Signatures.* Mol Cell, 2018. **72**(2): p. 250-262 e6.
79. Ibuki, Y., M. Shikata, and T. Toyooka, *gamma-H2AX is a sensitive marker of DNA damage induced by metabolically activated 4-(methylnitrosamino)-1-(3-pyridyl)-1-butanone.* Toxicol In Vitro, 2015. **29**(7): p. 1831-8.
80. Hauer, M.H. and S.M. Gasser, *Chromatin and nucleosome dynamics in DNA damage and repair.* Genes Dev, 2017. **31**(22): p. 2204-2221.
81. Chassot, A., et al., *Radiotherapy with concurrent and adjuvant temozolomide in children with newly diagnosed diffuse intrinsic pontine glioma.* J Neurooncol, 2012. **106**(2): p. 399-407.
82. Fontanilla, H.P., et al., *Palliative reirradiation for progressive diffuse intrinsic pontine glioma.* Am J Clin Oncol, 2012. **35**(1): p. 51-7.
83. Hoffman, L.M., et al., *Clinical, Radiologic, Pathologic, and Molecular Characteristics of Long-Term Survivors of Diffuse Intrinsic Pontine Glioma (DIPG): A Collaborative Report From the International and European Society for Pediatric Oncology DIPG Registries.* J Clin Oncol, 2018. **36**(19): p. 1963-1972.
84. Khuong-Quang, D.A., et al., *K27M mutation in histone H3.3 defines clinically and biologically distinct subgroups of pediatric diffuse intrinsic pontine gliomas.* Acta Neuropathol, 2012. **124**(3): p. 439-47.
85. Castel, D., et al., *Histone H3F3A and HIST1H3B K27M mutations define two subgroups of diffuse intrinsic pontine gliomas with different prognosis and phenotypes.* Acta Neuropathol, 2015. **130**(6): p. 815-27.
86. Nagaraja, S., et al., *Histone Variant and Cell Context Determine H3K27M Reprogramming of the Enhancer Landscape and Oncogenic State.* Mol Cell, 2019. **76**(6): p. 965-980 e12.
87. Coppe, J.P., et al., *The senescence-associated secretory phenotype: the dark side of tumor suppression.* Annu Rev Pathol, 2010. **5**: p. 99-118.
88. Krajewska, M., et al., *Dynamics of expression of apoptosis-regulatory proteins Bid, Bcl-2, Bcl-X, Bax and Bak during development of murine nervous system.* Cell Death Differ, 2002. **9**(2): p. 145-57.

89. Elmore, S., *Apoptosis: a review of programmed cell death.* Toxicol Pathol, 2007. **35**(4): p. 495-516.
90. Westphal, D., R.M. Kluck, and G. Dewson, *Building blocks of the apoptotic pore: how Bax and Bak are activated and oligomerize during apoptosis.* Cell Death Differ, 2014. **21**(2): p. 196-205.
91. Azimian, H., et al., *Bax/Bcl-2 expression ratio in prediction of response to breast cancer radiotherapy.* Iran J Basic Med Sci, 2018. **21**(3): p. 325-332.
92. Khor, L.Y., et al., *Bcl-2 and Bax expression predict prostate cancer outcome in men treated with androgen deprivation and radiotherapy on radiation therapy oncology group protocol 92-02.* Clin Cancer Res, 2007. **13**(12): p. 3585-90.
93. Wang, P.G., et al., *Lower expression of Bax predicts poor clinical outcome in patients with glioma after curative resection and radiotherapy/chemotherapy.* J Neurooncol, 2019. **141**(1): p. 71-81.
94. Skene, P.J. and S. Henikoff, *An efficient targeted nuclease strategy for high-resolution mapping of DNA binding sites.* Elife, 2017. **6**.
95. Nakazawa, Y., et al., *Cooperative interaction between ETS1 and GFI1 transcription factors in the repression of Bax gene expression.* Oncogene, 2007. **26**(24): p. 3541-50.
96. van der Meer, L.T., J.H. Jansen, and B.A. van der Reijden, *Gfi1 and Gfi1b: key regulators of hematopoiesis.* Leukemia, 2010. **24**(11): p. 1834-43.
97. Du, P., et al., *GFI1 is repressed by p53 and inhibits DNA damage-induced apoptosis.* PLoS One, 2013. **8**(9): p. e73542.
98. Anastas, J.N., et al., *Re-programing Chromatin with a Bifunctional LSD1/HDAC Inhibitor Induces Therapeutic Differentiation in DIPG.* Cancer Cell, 2019. **36**(5): p. 528-544 e10.